ACS OMEGA

http://pubs.acs.org/journal/acsodf
Mini-Review

Porphyrin-Based Hole-Transporting Materials for Perovskite Solar Cells: Boosting Performance with Smart Synthesis

Published as part of ACS Omega virtual special issue "At the Speed of Light: Recent Advances in Optoelectronics".

Melani J. A. Reis, Ana M. V. M. Pereira,* Nuno M. M. Moura,* and Maria G. P. M. S. Neves*

Cite This: *ACS Omega* 2024, 9, 31196−31219

ABSTRACT: Perovskite solar cells (PSCs) are becoming a promising and revolutionary advancement within the photovoltaic field globally. Continuous improvement in efficiency, straightforward processing methods, and use of lightweight and cost-effective materials represent superior features, among other notable aspects. Still, long-term stability and durability are issues to address to facilitate widespread commercial adoption and practical application prospects. Research has focused on overcoming these challenges, and charge transport materials play a critical role in determining charge dynamics, photovoltaic performance, and device stability. Conventional hole-transporting materials (HTMs), spiro-OMeTAD and PTAA, contribute to remarkable power conversion efficiencies owing to high thin-film quality and matched energy alignment. However, they often show a high material cost, low carrier mobility, and poor stability, which greatly limit their practical applications. Now, this review outlines recent advances in synthetic approaches to porphyrin-based HTMs to tune the charge dynamics by optimizing their molecular structures and properties. The main structural features comprise porphyrins of A_4-type, *trans* A_2B_2-type, and photosynthetic pigment analogues. Strategies include well-established routes to provide the required macrocycles, such as condensation of pyrrole or dipyrromethanes with suitable aldehydes, metalation of the porphyrin inner core, and postfunctionalization of peripheral positions. These functionalizations involve conventional procedures (e.g., halogenation, esterification, transesterification, nucleophilic oxidation, reduction, and nucleophilic substitution) as well as metal-catalyzed ones such as Suzuki−Miyaura, Sonogashira, Buchwald−Hartwig, and Ullmann cross-coupling reactions. As HTMs can also protect the perovskite layer from the external environment, porphyrin structures play a pivotal role in chemical, mechanical, and environmental stability, with their high hydrophobicity ability as the most significant parameter. The impact of porphyrins on the hole hopping of other HTMs while acting as an additive or an interlayer, passivating defects, and improving charge transport is also highlighted to provide real insights into ways to develop efficient and stable porphyrin-based materials for PSCs. This perspective aims to guide the scientific community in the design of new porphyrin molecules to place PSCs as an outperformer in photovoltaic technologies.

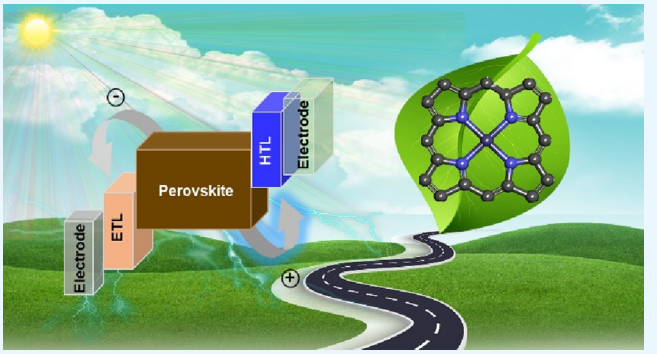

INTRODUCTION

Nowadays, it is unquestionable that the current social context based on rapid economic development results in the global greenhouse effect, the fossil energy crisis, environmental pollution, and generic respiratory diseases, among others. To overcome all this, reducing carbon dioxide emissions and achieving the objective of carbon neutrality have become inevitable for the desired transition to green and more sustainable development.

As such, exploiting and developing photovoltaic power generation technologies that enable efficient conversion and storage of solar energy is an effective measure.[1] In more recent years, the scientific research focus has been on perovskite solar cells (PSCs), first reported by Myasaka et al. in 2009.[2] In this pioneering investigation, methylammonium lead halide $CH_3NH_3PbI_3$ was applied as the active material to replace the organic dyes in dye-sensitized solar cells (DSSCs), achieving a power conversion efficiency (PCE) of 3.8%. In 2012, Park et al. revolutionized the field by replacing the polar liquid electrolyte with the solid-state 2,2′,7,7′-tetrakis[*N*,*N*′-

Received: February 28, 2024
Revised: June 15, 2024
Accepted: June 19, 2024
Published: July 9, 2024

di(4-methoxyphenyl)amino]-9,9′-spirobifluorene (spiro-OMeTAD, Figure 1), resulting in a PCE of 9.7%. Now, in 2024, the

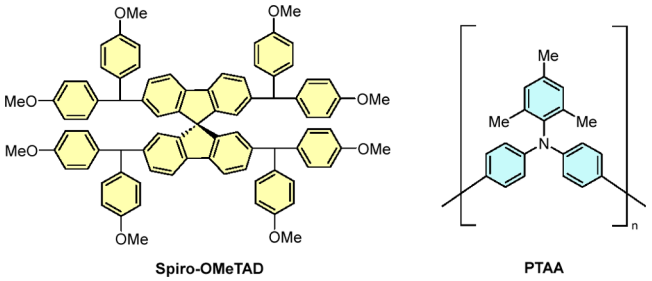

Figure 1. Chemical structures of spiro-OMeTAD and PTAA.

certified PCE is 26.1% and is already not far from the theoretical Shockley-Queisser limit of 33.7% using a single-junction solar cell.[3]

Perovskites exhibit outstanding optoelectronic properties, including high absorption coefficients, low recombination ratios, high charge mobilities, and tunable band gaps, contributing to their success in solar cells. The low cost, concise device structure, and straightforward fabrication methods also enhance their appeal.[4] The challenge of constructing large-area devices, crucial for commercialization, requires addressing perovskite material degradation from external factors like water, light, and temperature as well as internal factors such as defects and ion migration.[5] The layers in contact with the active perovskite layer, specifically the electron-transporting layer (ETL) and the hole-transporting layer (HTL), play a vital role in determining device performance and long-term stability (Figure 2). Perovskite solar cells come in conventional (n-*i*-p) and inverted (p-*i*-n) structures, with mesoporous or planar architectures based on the bottom transport layer morphology (Figure 2). Despite the differed configuration of these structures, the HTL is crucial for efficient charge conduction and suppression of charge recombination for all of them.[4,5] The hole-transporting material (HTM) must possess specific characteristics including compatible energy levels, adequate hole mobility, high stability and processability, and cost-effectiveness.

Spiro-OMeTAD, the first HTM, remains widely used, especially in n-*i*-p devices, due to its thermal stability and solubility as well charge-transporting ability. Nonetheless, low conductivity and poor hole mobility require frequent dopants and additives, affecting long-term stability. Moreover, the complex synthesis and low yield turn spiro-OMeTAD economically unviable. The polymer (poly[bis(4-phenyl)-(2,4,6-trimethylphenyl)amine] (PTAA, Figure 1) is now a promising HTM contributing to PCE over 23%. But issues such as the presence of polymeric chains with undefined chemical structures and variable molecular weights compromise its reliability and reproducibility in properties as well as device performance. Researchers are exploring alternative HTMs with simplified synthesis and enhanced performance and stability.[6]

Among them, porphyrins are well-known for their biological relevance in vital functions such as oxygen transport, photosynthesis, and enzymatic reactions and are meriting special attention from the scientific community. These compounds exhibit strong absorption in the visible region and are key components in light-harvesting antenna complexes in natural photosynthetic systems. They also participate in charge separation and electron transfer processes, offer excellent thermal and chemical stability, and are resistant to solar irradiation.[7] Naturally, the utilization of these macrocycles in energy-related fields was rapidly foreseen, and PSCs were not an exception. In 2016, conjugates comprising Zn(II) complexes of porphyrins with appended ethynylaniline entities were used for the first time as the HTM in PSCs generating a PCE of 16.6%.[8] Since then, porphyrins have been extensively studied as HTM, with a maximum PCE of 22.67% achieved in 2022,[9] and have already been reviewed by several authors.[10−12] However, there is an obvious need for a comprehensive analysis of the synthetic strategies to reach structural optimization of porphyrin-based HTMs and the influence of molecular structures on both PCE and chemical and environmental device stabilities. Moreover, considering the current sophisticated doping compositions of HTMs, porphyrins are easily dissolved into the perovskite solution or

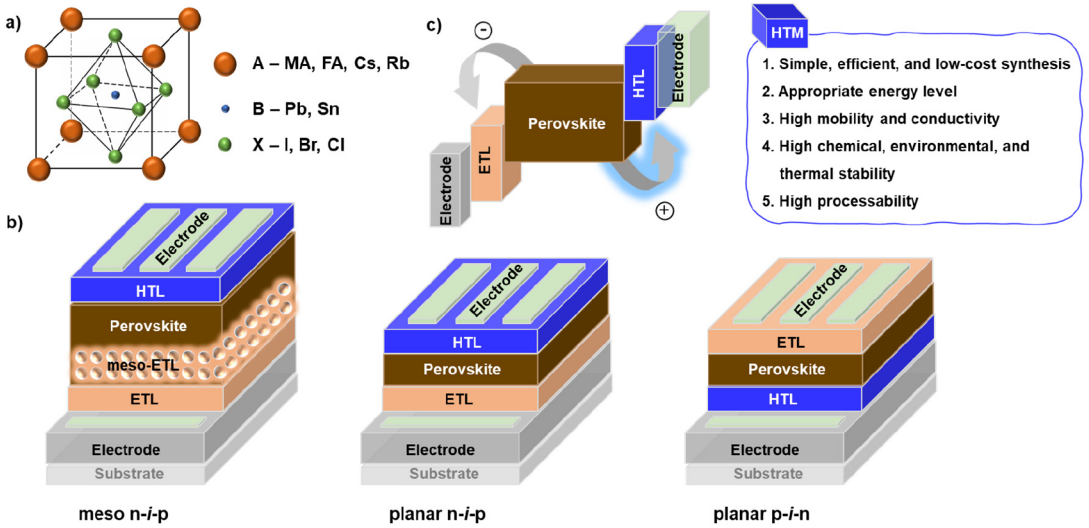

Figure 2. (a) Structure of a perovskite crystal (MA is methylammonium $[CH_3NH_3]^+$, and FA is formamidinium $[CN_2H_5]^+$), (b) device architecture of perovskite solar cells, and (c) schematic representation of charge transport and reference to ideal HTM features.

https://doi.org/10.1021/acsomega.4c01961
ACS Omega 2024, 9, 31196−31219

Scheme 1. Synthetic Approaches to the Aldehyde A1, Porphyrin 1, and Its Cu(II), Zn(II), and Co(II) Complexes

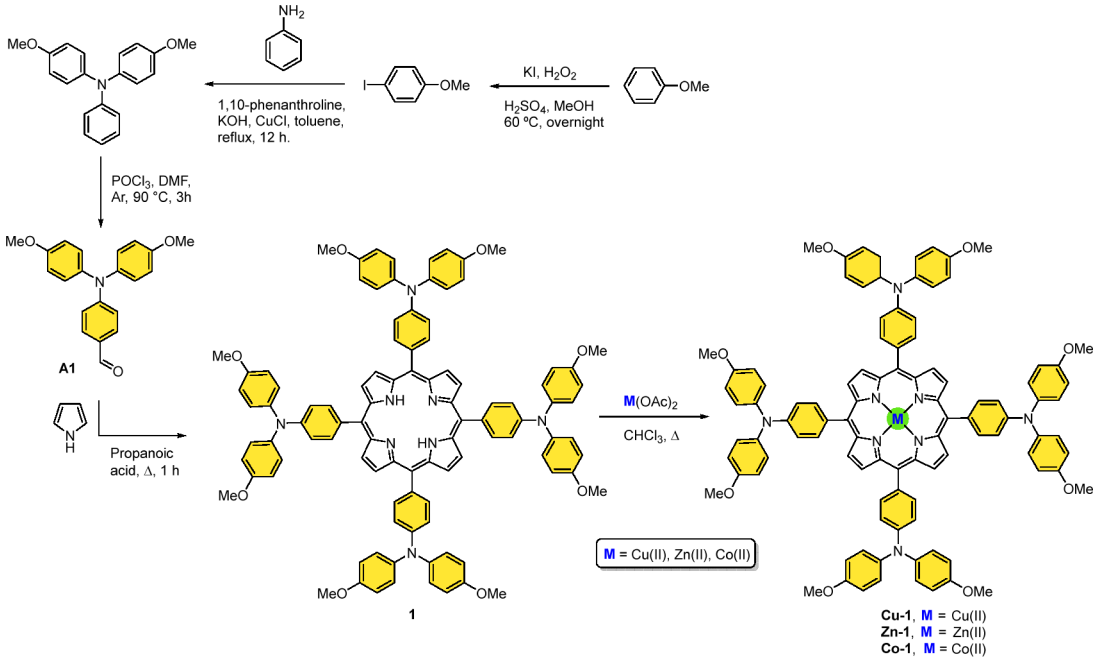

antisolvent to improve the crystal morphology to passivate defects as well as the stability of the perovskite material. The structural peculiarity is the presence of heteroatoms (O, S, and N) in the substituents, which allow stronger interactions with the perovskite layer and passivation of defects through interactions with the bare ions of the crystal structure. Additionally, acting as an interfacial modification layer, porphyrins not only passivate defects but also contribute to the transport of holes from the perovskite layer to the active HTM and improve stability toward humidity.

The scope of this review is to summarize recent advances made in the structural optimization of porphyrin-HTMs and to engineer doping composition or layers to guide further innovations in designing cheap, efficient, and stable HTMs for future applications.

To facilitate the discussion, the survey will start by referring to the synthetic strategies that afford HTMs based on symmetrical 5,10,15,20-tetraarylporphyrins (A_4 type), followed by those with structures of the *trans*-A_2B_2 type. The remaining sections will be dedicated to HTMs obtained via postfunctionalization of 5,15-diarylporphyrins (*trans*-A_2 type) at the free *meso*-positions and of photosynthetic pigments. Finally, attention will also be given to approaches to afford porphyrins acting as defect passivators, incorporated into the perovskite layer, or as interfacial material, while enhancing the hole extraction capability.

A_4-type PORPHYRINS AS HTMs

The possibility of exploring symmetrical 5,10,15,20-tetraarylporphyrins as HTM has been considered by several groups, after the promising results reported in 2017 by Zhu and coworkers (Scheme 1).[13] These macrocycles, with an A_4-type core, can be considered attractive targets due to the ready availability in a few synthetic steps and as most of the reagents are commercially available or require minimal handling.

In this first work, the efficiency of 5,10,15,20-tetrakis{4-[*N*,*N*-di(4-methoxylphenyl)aminophenyl]}porphyrin **1** coordinated with Zn(II) or Cu(II) metal ions was evaluated in standard devices with the following layers: FTO/compact TiO_2/mesoporous TiO_2/$MAPbI_3$/HTM/Au (Scheme 1). The starting scaffold **1** was obtained in 22% yield from the condensation of 4-[bis(4-methoxyphenyl)amino]benzaldehyde and pyrrole in refluxing propanoic acid according the conditions reported by Adler and Longo for the Rothemund reaction.[14] The required complexes **Cu-1** and **Zn-1** were obtained quantitatively after complexation of scaffold **1** with $Cu(OAc)_2$ and $Zn(OAc)_2$, respectively (Scheme 1).[15] The aldehyde, although commercially available, was prepared by iodination of methoxybenzene followed by copper-catalyzed Ullmann coupling with aniline and then formylation of the 4-methoxy-*N*-(4-methoxyphenyl)-*N*-phenylbenzenamine under Vilsmeier conditions ($DMF/POCl_3$).[16]

The photovoltaic performance showed the superiority of the Zn(II) complex when compared with the Cu(II) complex (PCE = 17.78% versus 15.36%), and the PCE was even comparable to the one obtained for spiro-OMeTAD (18.59%) under similar conditions. The lower performance of **Cu-1**, despite the deeper HOMO level than **Zn-1**, was attributed to its low solubility in the film preparation solvent (chlorobenzene), leading to irregular surfaces and pinholes, causing undesirable fast charge recombination. Interestingly, stability studies over 30 days at ambient conditions (around 20 °C and 40% humidity) showed that devices based on **Zn-1** maintained 85% of the initial PCE, while spiro-OMeTAD-based devices retained only 45% of their initial PCE value.

Posteriorly, the efficiencies of the free-base 5,10,15,20-*tetrakis*{4-[*N*,*N*-di(4-methoxylphenyl)amino-phenyl]porphyrin **1** and of the corresponding Co(II) complex **Co-1** (Scheme 1) were also evaluated as HTM in PSC devices with a p−*i*−n configuration, using the same $MAPbI_3$ perovskite.[17] The synthetic strategy differed from the previous strategy only in the coordination step that was performed in the presence of $Co(OAc)_2$. **Co-1** complex exhibited better photovoltaic performance than the free-base (PCE of 16.9% versus 14.5%), and this was ascribed to (i) better morphology of the perovskite layer when placed on top of the complex

https://doi.org/10.1021/acsomega.4c01961
ACS Omega 2024, 9, 31196−31219

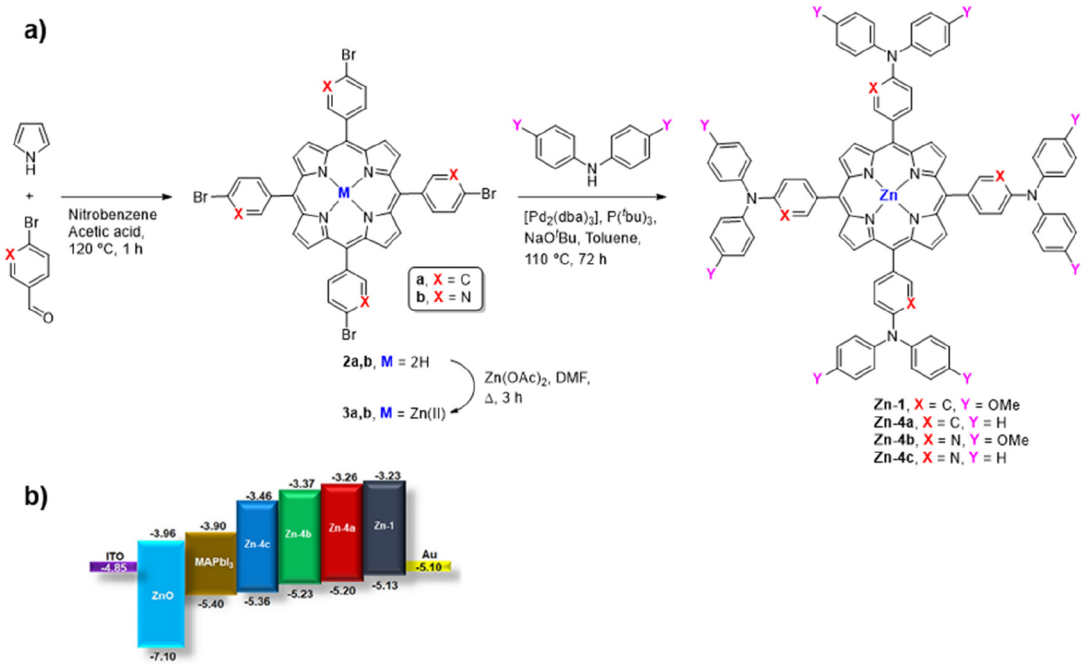

Figure 3. (a) Synthetic approach to Zn(II) complexes **Zn-1** and **Zn-4a−c** and (b) energy-level diagram of the Zn(II) complexes in PSC devices (figure adapted from ref 18 with permission from John Wiley and Sons).

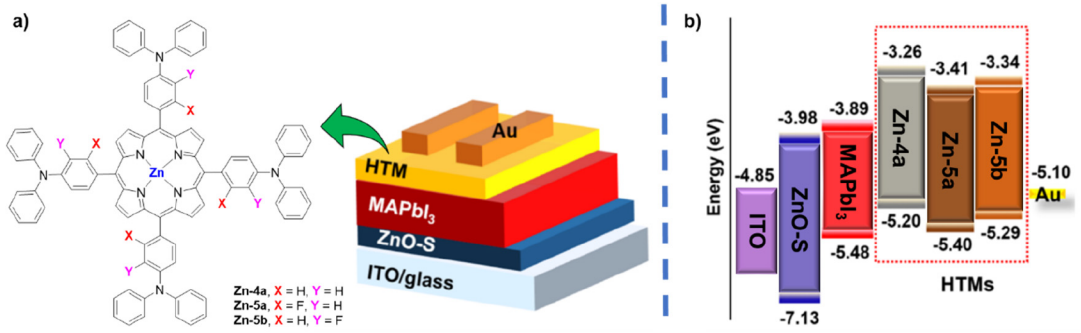

Figure 4. (a) Structure of PSC device and (b) energy-level diagram using complexes **Zn-4** and **Zn-5a,b** as the HTM (adapted from ref 19 Copyright 2018 American Chemical Society).

(improved crystallinity and higher contact angle); (ii) more suitable alignment of the HOMO level (−5.3 eV for **Co-1** and −5.03 eV for **1**) with the perovskite valence band (−5.4 eV) facilitating the extraction of holes. Although no PCE results were provided for devices constructed with the conventional HTM PTAA, the study showed that both porphyrins exhibit hole mobility values comparable to those of PTAA.

In another study, the efficiency of complexes **Zn-1** and **Zn-4a−c** (Figure 3) as HTM was compared using low-temperature processed PSCs. These molecules present structural differences in the unit directly linked to the porphyrin core (phenyl or pyridyl) and in the terminal arylamino substituents (**Y** = H or OMe), allowing to correlate their structures with photovoltaic efficiency.[18] The synthetic protocol involved the preparation of starting scaffolds **2a,b** by condensation of the appropriate aldehyde (4-bromobenzaldehyde or 2-bromopyridine-5-carboxaldehyde) with pyrrole under oxidative acidic conditions, followed by coordination with Zn(II) metal ion. Then, condensation of the resulting complexes **3a,b** was carried out with either diphenylamine or bis(4-methoxyphenyl)amine under Buchwald−Hartwig amination conditions (Figure 3a).

The study found that the HOMO energy level is influenced by the nature of the substructural units present in the porphyrin macrocycle, with the pyridine ring leading to a downshift, while the methoxy substituents lead to upshift. The best alignment with the perovskite active layer was found for the complex **Zn-4c** (Figure 3b), which presented a PCE value almost as good as that resulting from spiro-OMeTAD (14.11% versus 14.61%). The other devices displayed lower PCE values, varying between 11.96% for **Zn-4a** and 13.52% for **Zn-4b**. Devices fabricated with the porphyrinic HTM **Zn-4c**, principally undoped ones, showed higher stability than those made of spiro-OMeTAD. After 25 days, 92% of devices with **Zn-4c** maintained their initial performance, while for spiro-OMeTAD the value dropped to 6.1%, and only 73% of those were able to keep it.

In an effort to find cost-effective ways to produce efficient HTMs, the previous group reported the synthetic access to complexes **Zn-5a** and **Zn-5b** (Figure 4a) bearing fluorinated triphenylamine units at the four *meso*-positions; the study also considered the preparation of nonfluorinated **Zn-4a** for comparison purposes (Figure 4).[19] The envisioned synthetic strategy required the initial preparation of tetra-brominated

https://doi.org/10.1021/acsomega.4c01961
ACS Omega 2024, 9, 31196−31219

Scheme 2. Synthetic Approach to Complex Zn-6

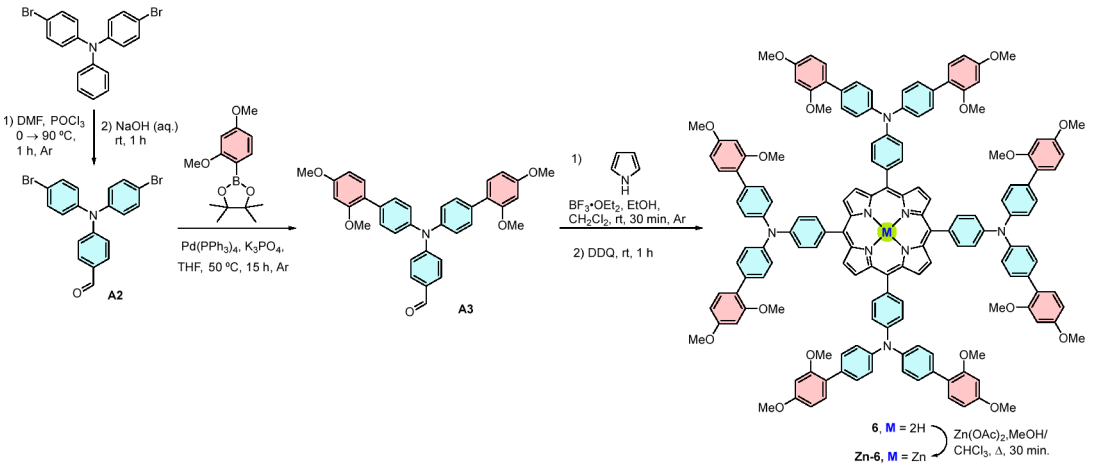

Scheme 3. Synthesis of Amine A4 and Its Coupling with Porphyrin 2a Followed by Metalation to Yield Complex Zn-7

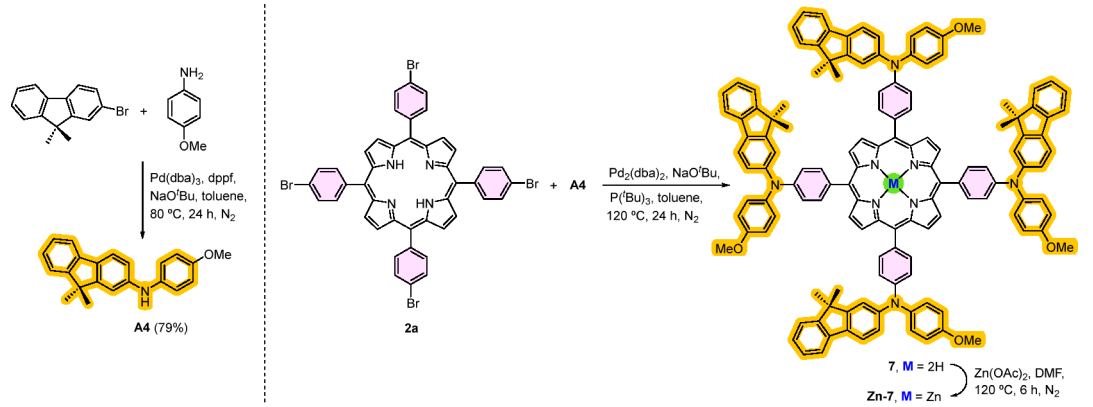

porphyrin free-base derivatives (~45%) by condensation of pyrrole with the adequate *p*-brominated aldehyde under oxidative acidic conditions [nitrobenzene plus acetic acid or under Lindsey conditions (reaction catalyzed by BF_3 and performed in the absence of oxygen and light followed by the oxidation step with DDQ)]. Metalation with $Zn(OAc)_2$ allowed the authors to reach the corresponding Zn(II) complexes in moderate to excellent yields (50−91%). The coupling of these complexes with diphenylamine under Buchwald−Hartwig conditions afforded the desired complexes **Zn-4a** (65%), **Zn-5a** (35%), and **Zn-5b** (30%).

The low-temperature processed PSCs using $MAPbI_3$ perovskite showed that the presence of the fluorine atom, mainly at position 2, has a positive effect on performance (Figure 4a). Complex **Zn-5a** contributed to a PCE of 18.85%, better than the value of 16.37% displayed by the non-fluorinated porphyrin **Zn-4a**. This improvement, especially when compared to the efficiency of **Zn-5b** (17.71%), was attributed to a more suitable HOMO level causing higher hole mobility (Figure 4b). Although the performance of devices based on **Zn-5a** using additives was slightly worse than that of spiro-OMeTAD (18.85% versus 19.23%), in their absence **Zn-5a** showed superior performance (14% versus 10%).

Macrocycle **6** and its Zn(II) complex **Zn-6** are other examples of porphyrins decorated at the four *meso*-positions with arylamines and with potential to be explored as HTM (Scheme 2).[20] The synthetic protocol involved the condensation of 4-(bis(2′,4′-dimethoxy-[1,1′-biphenyl]-4-yl)-amino)benzaldehyde (**A3**) with pyrrole in the presence of $BF_3{\cdot}O(Et)_2$ followed by oxidation with DDQ, according to Lindsey conditions.[21] The free-base **6**, obtained in 42% yield, was posteriorly metalated with $Zn(OAc)_2$ to afford **Zn-6** in 95% yield. However, the synthesis of aldehyde **A3** from 4-bromo-*N*-(4-bromophenyl)-*N*-phenylaniline required some investment (Scheme 2). The procedure involved the formylation of the amine under Vilsmeier−Haack conditions affording aldehyde **A2** (95%), which after Suzuki−Miyaura cross-coupling with the organoboron reagent 2-(2,4-dimethoxyphenyl)-4,4,5,5-tetramethyl-1,3,2-dioxaborolane gave the required aldehyde **A3** in 90% yield. The authors pointed out that condensation of this aldehyde with the pyrrole under Adler conditions led to a polymerization process and not to the desired macrocyclization. Probably due to the size of the aldehyde, the highly diluted conditions used in the Lindsey method are more favorable for porphyrinogen formation than the Adler conditions.

The study confirmed that the HOMO levels of **6** (−5.35 eV) and **Zn-6** (−5.37 eV) are adequate to be used as HTM in perovskite-based devices. Hole mobility values ($(5.18 \pm 0.5) \times 10^{-4}$ cm^2 V^{-1} S^{1-} and $(8.89 \pm 0.5) \times 10^{-4}$ cm^2 V^{-1} S^{1-} for **6** and **Zn-6**, respectively) analogous to spiro-OMeTAD ($(2.5 \pm 0.5) \times 10^{-4}$ cm^2 V^{-1} s^{-1}) were also observed. The authors expect to provide the PCE of PSC devices based on these HTMs in future work.

In 2022, Zhong and co-workers reported the synthetic access and efficiency as HTM of complex **Zn-7** bearing *meso*-

https://doi.org/10.1021/acsomega.4c01961
ACS Omega 2024, 9, 31196−31219

triarylamino moieties, each featuring a terminal fluorene (Scheme 3).[22] The key step was the C−N coupling between readily accessible 5,10,15,20-*tetrakis*(4-bromophenyl)-porphyrin **2a** and *N*-(4-methoxyphenyl)-9,9-dimethyl-9*H*-fluoren-3-amine **A4** under Buchwald−Hartwig conditions. After metalation of the resulting free-base derivative **7** with $Zn(OAc)_2$, required **Zn-7** was obtained in 66% yield. The Buchwald−Hartwig approach was also used to prepare amine **A4** from 2-bromo-9,9-dimethyl-9*H*-fluorene and *p*-anisidine.

The photovoltaic studies showed that $FAMAPbI_3$-based devices prepared with the fluorene complex **Zn-7** as the HTM are more efficient than those with **Zn-1** (Scheme 1), selected for comparison (19.31% versus 17.75%). This positive impact was mostly ascribed to the higher open-circuit voltage (V_{oc}) of 1.08 V when compared to that resulting from **Zn-1**, 0.97 V. Despite the slightly lower PCE than the spiro-OMeTAD (20.45%), **Zn-7** offers cost savings ($32 vs $91) and maintains thermal stability in nonencapsulated devices, retaining 97% of the initial efficiency after 20 days in low humidity conditions (5% humidity) and 73% after exposure at 85 °C for 55 h.

Zhong and co-workers also decided to evaluate the effectiveness of **Zn-4a** complex (Figure 4), after being electropolymerized, as a dopant-free HTM in inverted $MAPb(Cl_{0.05}I_{0.95})_3$ PSCs (Figure 5).[23] The **Zn-4a** complex

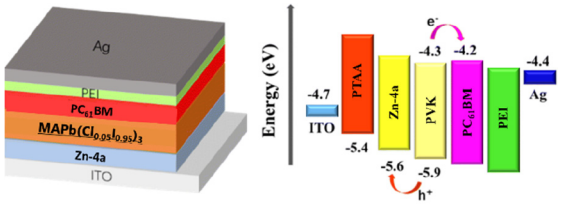

Figure 5. PSC device structure and energy-level diagram using the electropolymerized complex **Zn-4** as the HTM (figure adapted from ref 23 with permission from Royal Society of Chemistry).

was obtained in *ca.* 76% yield by reacting free-base **2a** with diphenylamine under Buchwald−Hartwig conditions, followed by the metalation step. The electropolymerization of **Zn-4a** was carried out using cyclic voltammetry, and the control of scan cycles between 2 and 25 afforded polymeric films with different thicknesses; the network resulted from the C−C coupling of cation radicals generated during the oxidative process. The best photovoltaic performance was reached for the film with 79 nm of thickness (PCE = 19.75%; V_{oc} = 1.10 V, J_{sc} = 22.40 mA cm^{-2}, and FF = 80.09%). Nonencapsulated devices retained 70% of their initial efficiency for 20 days after thermal aging at 85 °C in a nitrogen glovebox. In comparison, PSCs based on PTAA showed a 78% decrease in the initial efficiency (19.12%). Furthermore, after 208 days in a glovebox, 96% of the initial PCE was maintained for **Zn-4a**-based devices, while only 40% was retained in PTAA-based cells.

Porphyrin derivatives functionalized with acylhydrazone groups have demonstrated excellent charge transport properties.[24] Thus, Liu and co-workers evaluated the efficiency of the complex **Zn-10**[25] and later of the corresponding Cu(II) complex **Cu-10**[26] as HTM in PSCs. The devices followed the conventional mesoporous configuration of $FTO/TiO_2/MAPbI_3$/HTM/Au (Scheme 4).

The access to **Zn-10** and **Cu-10** required the reaction between the Zn(II) or Cu(II) complexes of 5,10,15,20-tetrakis(4-methoxycarbonylphenyl)porphyrin **8** (prepared using Lindsey conditions) with hydrazine hydrate and then the condensation of the obtained hydrazide complexes **Zn-9** or **Cu-9** with 2-pyridinecarboxaldehyde.

Both complexes exhibited higher HOMO energy levels (−5.12 eV and −5.35 eV for **Cu-10** and **Zn-10**, respectively) compared to $MAPBI_3$ perovskite (−5.43 eV), ensuring the required driving force for hole injection from the perovskite into the Au electrode. Photovoltaic results revealed that PSC devices using **Cu-10** as the HTM outperformed those based on **Zn-10** (PCE of 18.21% vs. 17.82%). This superior performance was attributed to a slightly higher J_{SC} (22.57 mA cm^{-2} for **Cu-10** and 22.29 mA cm^{-2} for **Zn-10**) and also to the redox shuttle between the Cu(I) and Cu(II) centers in **Cu-10**, which makes it more suited than **Zn-10** as HTM. Although the performance of **Cu-10** was slightly lower than that of spiro-OMeTAD (PCE = 18.6%), the porphyrinic HTMs resulted in better thermal, moisture, and illumination stability once again.

5,15-A_2B_2-type PORPHYRINS AS HTMs

Research in 5,10,15,20-tetraarylporphyrins with different substituents at the *meso*-positions typically focuses on those containing two different substituents in opposite positions. These macrocycles, known as *trans*-A_2B_2 or 5,15-A_2B_2 porphyrins, are generally synthesized by condensation of suitable dipyrromethanes and aldehydes followed by an oxidative step based on the approach developed by Lindsey and co-workers.[27]

In 2018, Coutsolelos and collaborators selected 5,15-A_2B_2 porphyrins **11a** and **11b** (Scheme 5) to explore the potential of free-base porphyrins as HTM in PSCs, using the n-*i*-p mesoscopic glass/FTO/TiO_2/$CH_3NH_3PbI_{3-x}Cl_x$/HTM/Au configuration.[28]

The synthetic procedure involved the condensation of 5-(4-carbomethoxyphenyl)dipyrromethane with 4-(dimethylamino)benzaldehyde in the presence of TFA, followed by oxidation with *p*-chloranil to afford porphyrin **11a** (15%), bearing ester functionalities. The hydrolysis of the ester groups under basic conditions yielded the acid porphyrin **11b** in 85%.

Both compounds showed HOMO energy levels like that of spiro-OMeTAD (−5.2 eV) and, thus, suitably aligned to provide efficient hole injection from the perovskite into the Au electrode. The superior photovoltaic performance of **11b**-based devices compared to **11a** (7.01% vs. 2.01%) was mainly attributed to film quality. Compound **11b** presents a smoother and more extensive surface coverage compared to the nanoflakes in the **11a**-film, compromising the contact with the perovskite and, consequently, charge transport. The discrepancy in film morphology was explained by the presence of the carboxy groups in **11b** promoting intermolecular hydrogen bonds and by the low solubility of **11a** in organic solvent ($CHCl_3$), which was used in the film preparation. Although the cells that incorporated **11b** showed a similar J_{sc} (23 mA cm^{-2}) to those based on spiro-OMeTAD, the lower V_{oc} (628 mV vs. 828 mV) and FF (0.49 vs. 0.82) can explain the higher PCE displayed by the reference (11.72%).

To improve PSCs stability against thermic, UV, and interfacial damage, Cao and co-workers selected the natural product sinapoyl malate (SM) with sunscreen features to modify the surface of the TiO_2 layer in devices with the A_2B_2 complexes **Co(II)-13**, **Co(III)-13**, and **Zn-13** as the HTM (Scheme 6 and Figure 6).[29] In selecting *meso*-substituents, the authors considered the donor features of methoxytriphenyla-

https://doi.org/10.1021/acsomega.4c01961
ACS Omega 2024, 9, 31196−31219

Scheme 4. Synthetic Access to Zn-10 and Cu-10 Complexes Used as HTM and Corresponding Energy-Level Diagram[a]

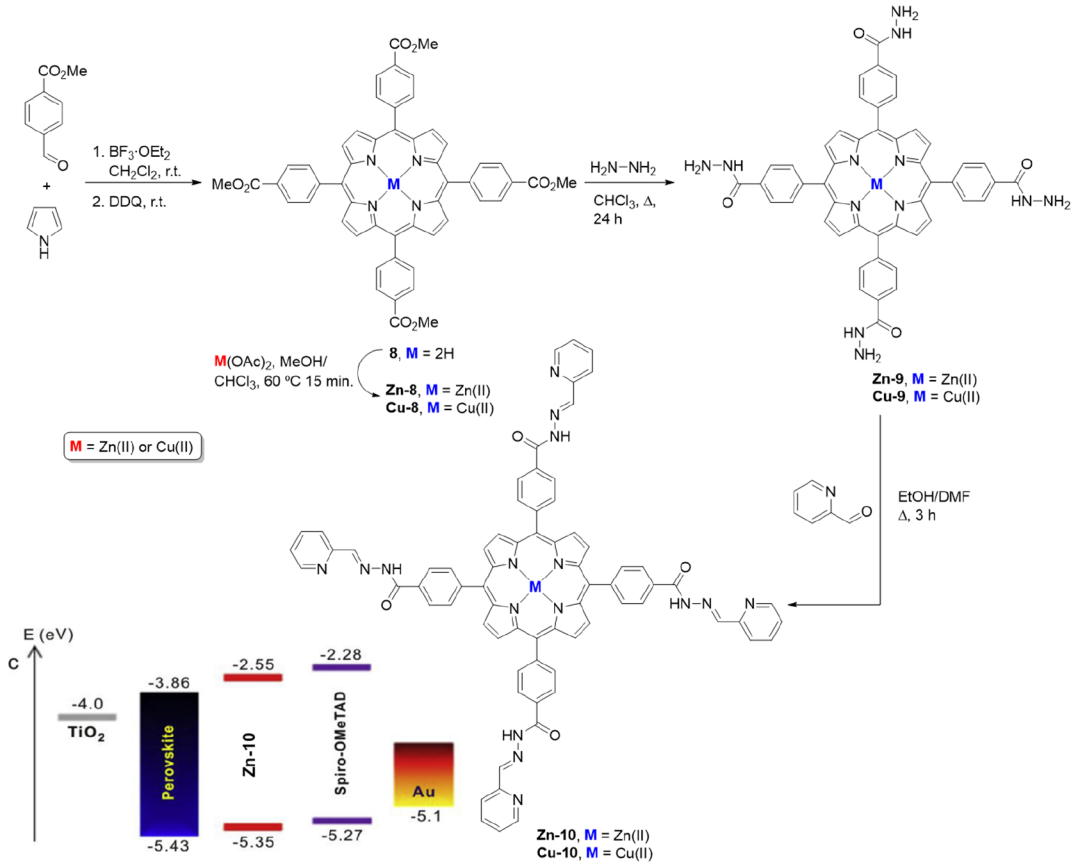

[a]Adapted from reference 25 with permission from Elsevier.

Scheme 5. Synthetic Approach to Yield the Ester and Acid Porphyrins 11a and 11b

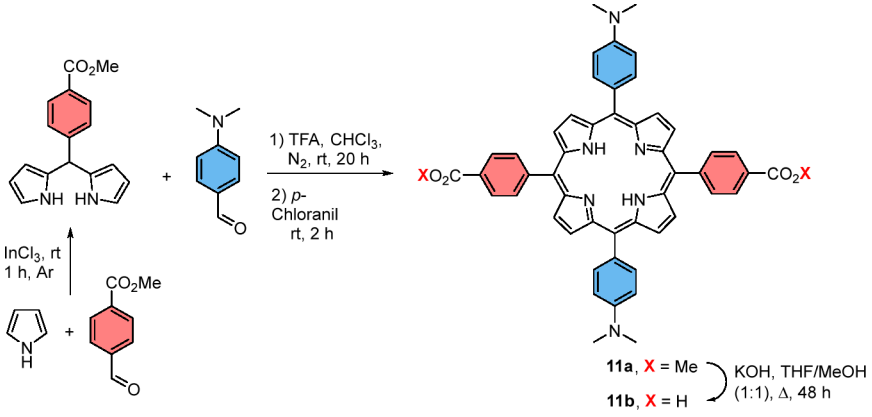

mino units to achieve efficient charge transport. Solubility in common organic solvents was assured by aryl groups substituted with methoxy/oxyalkyl chains. The preparation of free-base porphyrin **13** (25%) involved the condensation of dipyrromethane **12** with aldehyde **A1** under Lindsey conditions. The reaction of **13** with $Co(OAc)_2$ or $Zn(OAc)_2$ afforded the corresponding **Co(II)-13** (75%) and **Zn-13** (97%) complexes. **Co(III)-13** was obtained in 91% yield by air oxidation of **Co(II)-13** in the presence of HCl for 2 days.

The best photovoltaic performance, similar to spiro-OMeTAD, was achieved when a mixture of **Co(II)-13** and **Co(III)-13** complexes was used as the HTM. The study confirmed that devices with **Co(II)-13**/**Co(III)-13** exhibited high thermal stability and no significant morphological changes after heating above 80 °C, unlike spiro-OMeTAD, where ion diffusion of I^- and MA^+ ions from the $(CsFAMA)Pb(BrI)_3$ perovskite to the spiro-OMeTAD layer occurred. Furthermore, the SM interfacial modification successfully resolved the UV stability and reduced the poor interfacial contact between TiO_2 and perovskite.

HTMs OBTAINED Via POSTFUNCTIONALIZATION OF 5,15-A_2-PORPHYRINS

Porphyrins **14a–i** substituted at the 5,15-*meso* positions are effective scaffolds for further modifications to attain porphyrin

https://doi.org/10.1021/acsomega.4c01961
ACS Omega 2024, 9, 31196–31219

Scheme 6. Synthesis of Porphyrin 13 and of Its Zn(II), Co(II), and Co(III) Complexes

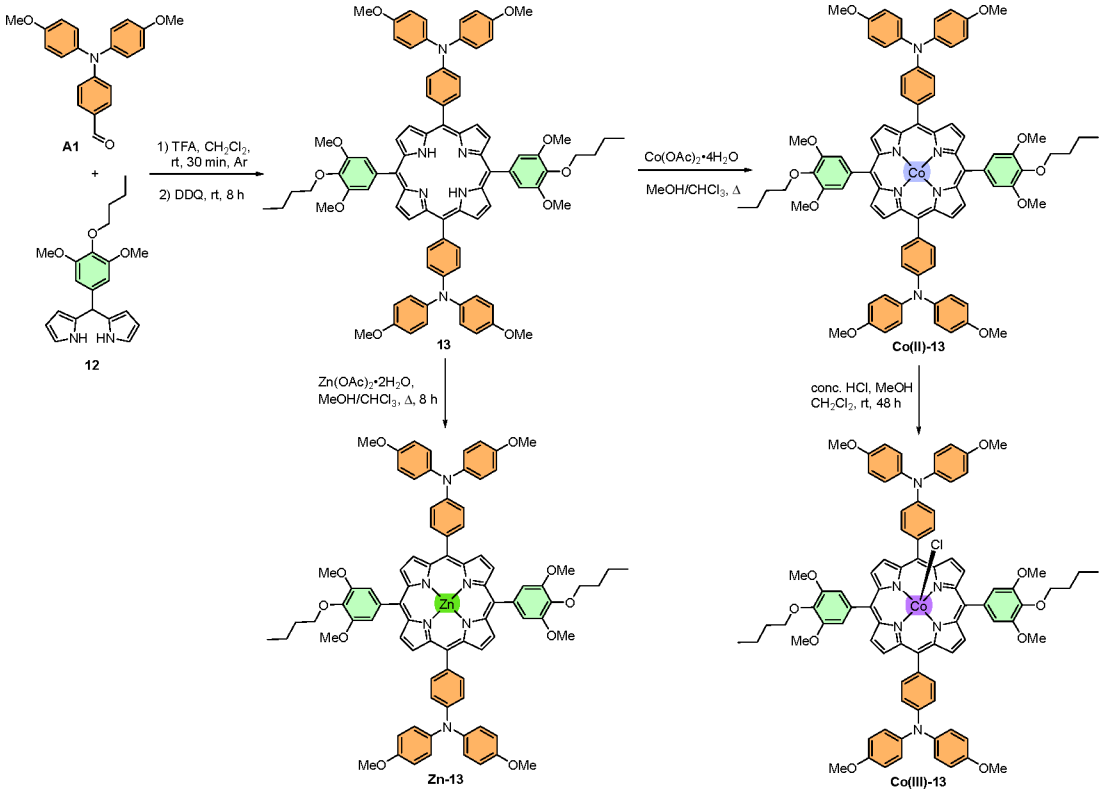

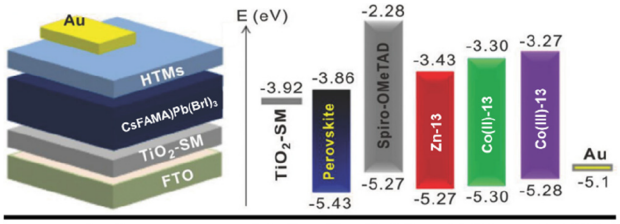

Devices	J_{sc}(mA·cm^{-2})	V_{oc} (V)	FF (%)	PCE (%)
TiO_2-SM/Spiro-OMeTAD	23.52	1.12	76.01	20.02
TiO_2-SM/**Zn-13**	23.15	1.12	73.39	19.03
TiO_2-SM/**Co(II)-13**	23.17	1.09	74.31	18.77
TiO_2-SM/**Co(III)-13**	23.16	1.09	70.88	17.88
TiO_2-SM/**Co(II)-13**/**Co(III)-13**	23.62	1.13	76.66	20.47

Figure 6. Device architechture, energy-level diagram, and photovoltaic parameters of TiO_2−SM-based mesoporous PSCs (figure adapted from ref 29 with permission from John Wiley and Sons).

macrocycles with HTM features (Scheme 7). These porphyrins are typically synthesized by condensing 2,2′-dipyrromethane with an aldehyde under Lindsey conditions (Scheme 7),[27] an approach usually preferable since *meso*-substituted dipyrromethanes are somewhat unstable and tend to produce several polymeric byproducts. Next, 5,15-disubstituted porphyrins **14a−i** are frequently submitted to a metalation step with $Zn(OAc)_2$ and then to dibromination of the free *meso* positions (10 and 20) with *N*-bromosuccinimide (NBS) providing porphyrin derivatives **Zn-15a−i**. These derivatives are subjected to different modifications and, in general, mediated by transition-metal complexes.

In 2019, Zhang and co-workers conducted a study to assess the performance of the Zn(II) complex of scaffold **14a** (Scheme 7) and of dipyrromethene Zn(II) complex **18** (Scheme 8) as HTM. The latter was synthesized via coordination of dipyrromethene **17** with $Zn(OAc)_2$, resulting from the oxidation of dipyrromethane **16** with DDQ (Scheme 8).[30]

Both compounds showed similar optical and redox properties as well HOMO levels (−5.38 eV for **18** and −5.28 eV for **Zn-14a**). However, the π-extended conjugation and intermolecular $\pi-\pi$ stacking induced by the planar porphyrin unit resulted in an almost 2-fold increase in hole mobility and

Scheme 7. Synthetic Approach to Prepare 5,15-Disubstituted Porphyrin Scaffolds 14a−i and Zn15a−i

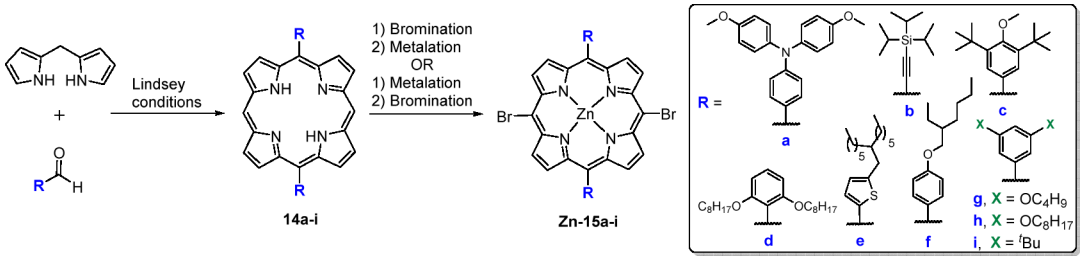

https://doi.org/10.1021/acsomega.4c01961
ACS Omega 2024, 9, 31196−31219

Scheme 8. Synthetic Approach to Prepare the Zn(II) Complex 18

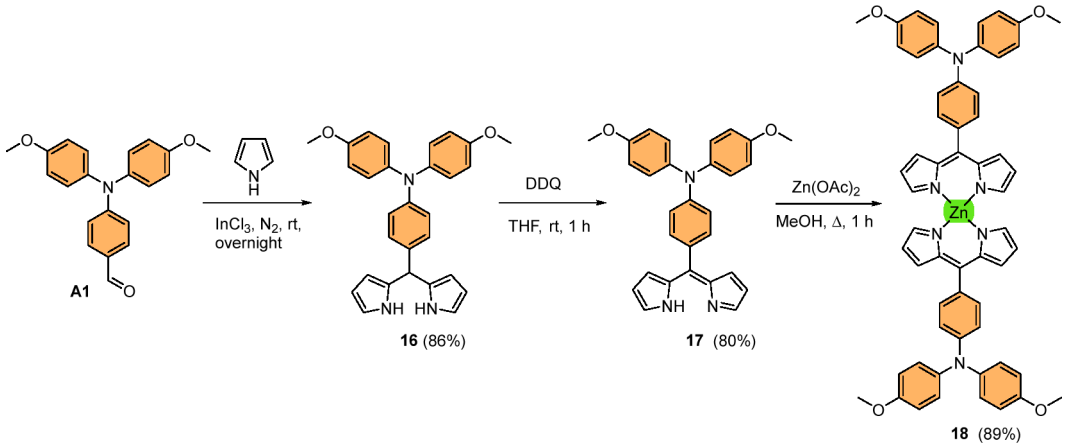

Scheme 9. Functionalization of 5,15-Diaryl Porphyrin with Dialkylaniline or Methylbenzoate Units

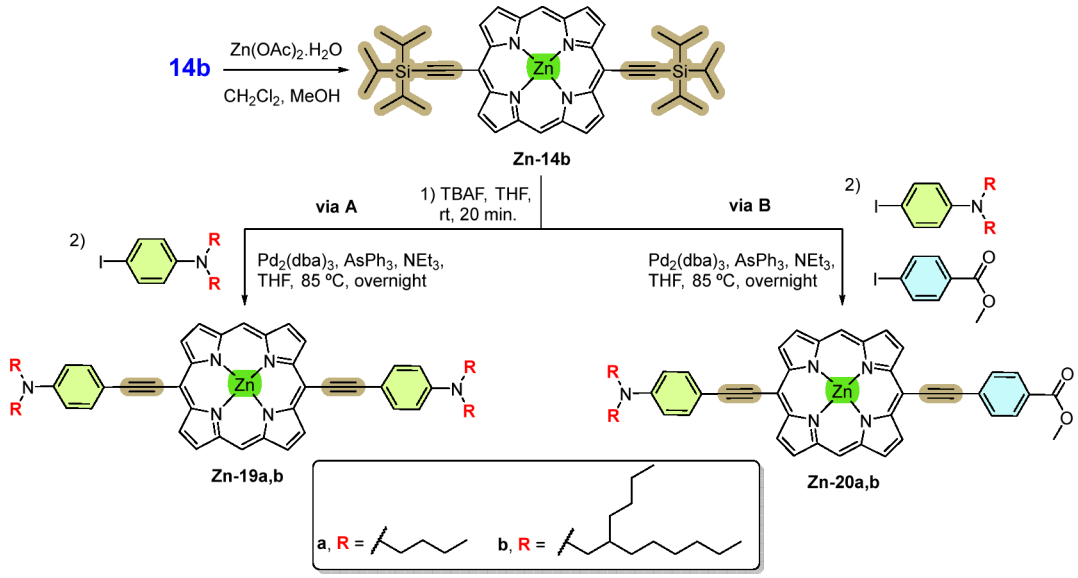

conductivity compared to that of **18**. As a result, in n-*i*-p mesocospic $(FA)_{0.85}(MA)_{0.15}Pb(I_3)_{0.85}(Br_3)_{0.15}$-based PSCs, **Zn-14a** contributed to a performance (16.05%) comparable to that of spiro-OMeTAD-based cells (17.08%). In contrast, devices made of **18** showed a negligible efficiency (0.01%). Stability tests showed that **Zn-14a** offers less stability than spiro-OMeTAD after 30 days in the dark at 25 °C and 50% humidity, which was related to the higher concentration of additives for **Zn-14a**.

Chou and co-workers evaluated the performance of the complexes **Zn-19a,b** and **Zn-20a,b**, also with no substituents at the *meso* positions as the HTM (Scheme 9).[31] The synthesis of these complexes, characterized by a one-dimensional linear structure, involved the initial base-promoted deprotection of silyl units at porphyrin **Zn-14b**, followed by Pd-mediated cross-coupling with *N,N*-dibutyl-4-iodoaniline or *N,N*-bis(2-butyloctyl)-4-iodoaniline, resulting in symmetrical push−push porphyrin-ethynylaniline derivatives **Zn-19a** (60%) and **Zn-19b** (42%) (Scheme 9, via A). Nonsymmetrical push−pull-type porphyrin derivatives **Zn-20a** (15%) and **Zn-20b** (16%) were prepared using the same synthetic approach but with an equimolar mixture of 4-iodo-*N,N*-dialkylaniline and methyl 4-iodobenzoate (Scheme 9, via B).

The devices obtained using the **Zn-19** and **Zn-20** series as HTM in mesoscopic layered FTO/TiO_2/$Cs_{0.05}[(FA_{0.83}MA_{0.17})PbI_{0.83}Br_{0.17}]_{0.95}$/HTM/Au PSCs resulted in a similar PCE of ∼15% for **Zn-20a** (14.95%), **Zn-20b** (14.50%), and **Zn-19a** (14.46%). In contrast, **Zn-19b** only contributed to a value of 5.81%. This poorer performance was ascribed to the lower hole mobility of the **Zn-19a**-based films and also to the worse surface morphology, highly affected by the bilateral functionalization with dialkylaniline branched chains. This impact was even more pronounced for undoped-HTMs devices, with PCE values of 12.10% for **Zn-19a** and 10.90% for **Zn-20a**, in contrast to the negligible value of 0.25% for **Zn-19b**. Even though spiro-OMeTAD HTM performed better than porphyrins in the presence of additives (PCE = 17.77%), stability studies carried out in the absence of them, in the dark with 40% humidity, showed that **Zn-20b** retains 85% of the initial PCE after 340 h, which is much better than that of spiro-OMeTAD.

However, it was the work developed by Chou and colleagues in 2016 that pioneered the exploration of A_2B_2-type Zn(II)-diaryl-porphyrins as HTM for PSCs.[8] The proposed molecules featuring ethynylaniline groups at *meso* positions were prepared starting by the Sonogashira cross-coupling of porphyrin **Zn-**

https://doi.org/10.1021/acsomega.4c01961
ACS Omega 2024, 9, 31196−31219

Scheme 10. Synthetic Route to Obtain Zn-22a,b by Sonogashira Coupling

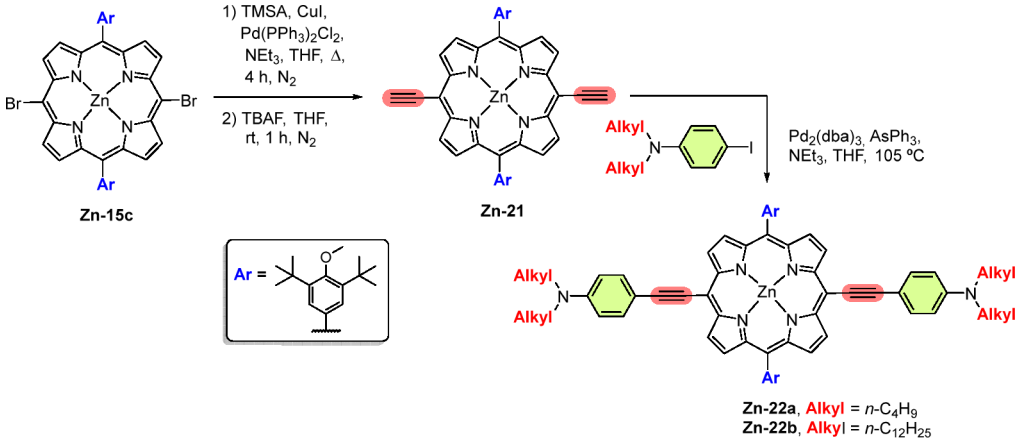

15c with trimethylsilylacetylene (TMSA) to yield the corresponding protected dialkynyl porphyrin derivative (70% yield). Subsequent removal of the protecting silyl groups through basic treatment with tetra-*n*-butylammonium fluoride (TBAF) allowed the isolation of porphyrin **Zn-21** (85%), with terminal alkyne groups in two *meso* positions, to undergo a Sonogashira cross-coupling reaction with the appropriate 4-iodo-*N*,*N*-dialkylaniline, affording **Zn-22a** (42%) and **Zn-22b** (49%) in moderate yields (Scheme 10).

Despite the HOMO levels of both porphyrins (−5.25 and −5.10 eV, respectively) were found to be very close to the HOMO level of spiro-OMeTAD (−5.22 eV), the hole mobility shown by **Zn-22b** is an order of magnitude lower (10^{-5} vs 10^{-4} cm^2 V^{-1} s^{-1}). As a result, **Zn-22a** contributed for a more favorable PCE than **Zn-22b** (16.60% vs 10.55%) in n-*i*-p mesoscopic $MAPbI_3$-based devices. In fact, the fewer pinholes observed in the perovskite layer for **Zn-22a** than for **Zn-22b** are a consequence of its shorter alkyl chains (*n*-butyl vs. *n*-dodecyl), leading to a V_{oc} (0.99 V), J_{sc} (22.82 mA cm^{-2}), and FF (0.73) like spiro-OMeTAD (V_{oc} = 1.06 V, J_{sc} = 22.79 mA cm^{-2}, FF = 0.74, PCE = 18.03%), in good agreement with the comparable hole mobility.

Later, Kang and collaborators selected complexes **Zn-23a−c** to evaluate how the photovoltaic performance was affected by the different *para*-substituted electron-donating diarylamine moieties (Figure 7).[32] The authors adapted the procedure

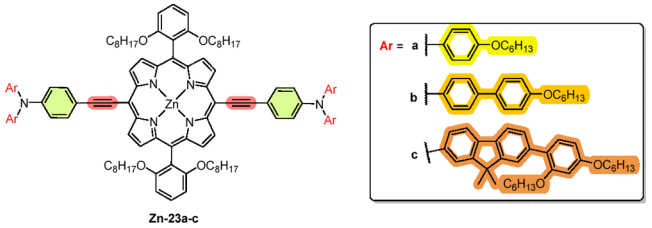

Figure 7. Chemical structures of complexes **Zn-23a−c**.

previously reported by Chou,[8] incorporating triisopropylsilane (TIPS) as a protective group instead. After TIPS removal, the resulting porphyrin undertook a Sonogashira cross-coupling reaction with the adequate aryl bromide derivative to give porphyrins **Zn-23a−c** in yields of around 32%.

Again, the HOMO energy level of developed porphyrins (−5.03 eV for **Zn-23a**, −5.27 eV for **Zn-23b**, and −5.05 eV for **Zn-23c**) were very similar to the HOMO energy level of spiro-OMeTAD (−5.25 eV) being located above the valence band (VB) of the $MAPBI_xCl_{3-x}$ perovskite (−5.43 eV). However, the evaluated hole mobility value for **Zn-23a** was higher (2.60×10^{-5} cm^2 V^{-1} s^{-1}) than those of **Zn-23b** (1.28×10^{-5} cm^2 V^{-1} s^{-1}) and **Zn-23c** (8.01×10^{-6} cm^2 V^{-1} s^{-1}). Indeed, **Zn-23a** with a less bulky donor enabled a tight molecular arrangement between molecules, increasing the $\pi-\pi$ stacking. In contrast, **Zn-23b** and **Zn-23c**, due to the larger dihedral angle between the alkoxy-substituted phenyl ring and the donor triarylamine core, compromised the dense molecular arrangement and the $\pi-\pi$ stacking. Furthermore, the study of the dynamic charge transfer process between the perovskite and the various HTM films showed that **Zn-23a** exhibited a more efficient hole extraction ability than **Zn-23b** and **Zn-23c**. In consequence, **Zn-23a**-based devices showed a PCE of 12.6%, while **Zn-23b** and **Zn-23c** contributed to performances of 11.5% and 9.0%, respectively.

Giribabu and co-workers employed the Sonogashira cross-coupling approach to synthesize *trans*-A_2B_2-type free-base porphyrin-ethynyl derivatives bearing *N*-octylphenothiazinyl or triphenylimidazolyl units as donor groups (Scheme 11).[33−35] The reaction of free-base porphyrin **15d** with terminal aryl alkynes derivatives, mediated by Pd(0) under conditions similar to those discussed for Zn(II) porphyrin derivatives, yielded free-base porphyrin derivatives **24** (85%) and **25** (79%). A notable distinction lies in the presence of bromine leaving groups at the porphyrin core and the ethynyl moiety at the phenoxazine and triphenylimizole units, as opposed to the inverse configuration in previously discussed works. This synthetic approach shows the advantage of eliminating additional sequential Sonogashira and deprotection steps to prepare the appropriate porphyrin-ethynyl derivatives.

Then, Zn(II) and Cu(II) complexes of the porphyrin derivatives **24** and **25** were prepared using standard metalation conditions in the presence of the appropriate acetate salt in a $MeOH/CHCl_3$ mixture (Scheme 11).

$MAPbI_3$-based devices incorporating porphyrin-based HTM **24** and **25** and their corresponding Zn(II) and Cu(II) complexes exhibited PCE values ranging from 9.12% to 12.85%, following the order free-base < Zn(II) < Cu(II). In contrast, the reference spiro-OMeTAD achieved a PCE value of 5.91%. The superior performance of Cu(II) complexes is attributed to lower activation energy, arising from a shorter bond length, and more pronounced $\pi-\pi$ stacking. Indeed, the better film formation in the device enhances conductivity and

https://doi.org/10.1021/acsomega.4c01961
ACS Omega 2024, 9, 31196−31219

Scheme 11. Synthesis of Free-Base Porphyrins 24 and 25 and Their Zn(II) and Cu(II) Complexes

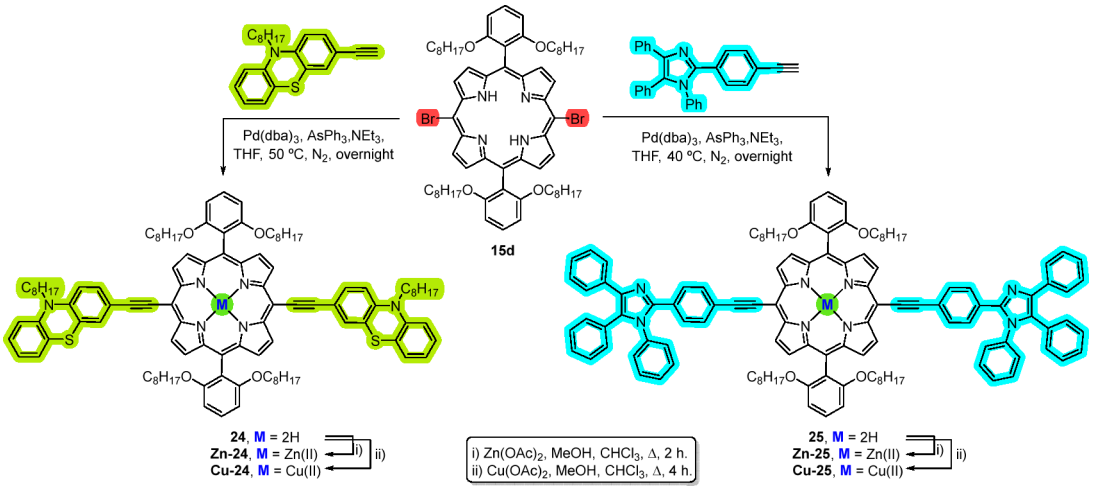

improves hole mobility. In addition, the hydrophobic nature of alkoxy chains resulted in a remarkable stability in water.

Gao and co-workers developed the acceptor−donor−acceptor (A−D−A) **Zn-26** featuring the central porphyrin core with 2-ethylhexylsulfidethienyl side chains as the donor and two diketopyrrolopyrrole moieties as the acceptor (Figure 8).[36] This molecule was employed as a bulk-heterojunction

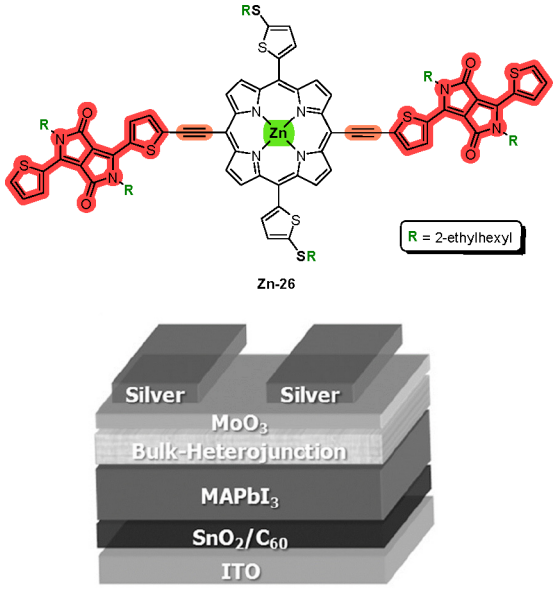

Figure 8. Chemical structure of **Zn-26** and architecture of the organic/perovskite hybrid solar cell used (figure adapted from ref 36 with permission from John Wiley and Sons).

(BHJ) layer on top of the $MAPbI_3$ perovskite to reach organic/perovskite hybrid solar cells with high near-infrared (NIR) photoresponse and a PCE of 19.02%. The synthetic approach involved the functionalization of the porphyrin **Zn-15e** scaffold (Scheme 7) through Sonogashira cross-coupling reaction with brominated thiophene-capped diketopyrrolopyrrole, under conditions adapted from those described by Chou,[8] resulting in the A−D−A porphyrin-derivative **Zn-26** in 68% yield.

The absorption spectrum of the **Zn-26** film exhibited broad coverage of the UV−vis-NIR spectrum with a maximum at 901 nm due to a strong electron delocalization along the enlarged π-conjugated system. The HOMO energy level of **Zn-26** (−5.20 eV) matches well the VB of $MAPbI_3$ perovskite (−5.4 eV) facilitating the hole extraction and transfer and helping to decrease the energy loss at the interfaces. The addition of $PC_{61}BM$ to **Zn-26** in the best ratio of 4:1 had also a positive impact in the hole mobility (increased from 3.2×10^{-5} to 1.6×10^{-4} cm^2 V^{-1} s^{-1}), ascribed to the improvement on film morphology.

The hybrid solar cells fabricated with a n-*i*-p planar configuration of $ITO/SnO_2:C_{60}/MAPbI_3/BHJ$ **Zn-26**:$PC_{61}BM/MoO_3/Ag$ (Figure 8) displayed a PCE value of 19.2%, with a V_{OC} of 1.04 V, J_{sc} of 23.32 mA cm^{-2}, and a FF of 0.78. Of note, the replacement of **Zn-26**:$PC_{61}BM$ by spiro-OMeTAD resulted in a lower PCE of 17.6%, coming from a lower J_{sc} (21.37 mA cm^{-2}) due to a photoresponse covering only from 380 to 800 nm, while the hybrid solar cells based on **Zn-26** also responded in the NIR region from 800 to 875 nm with ≈40% intensity.

In contrast, standard organic solar cells resulted in a maximum PCE of 7.83% (V_{oc} = 0.79, J_{SC} = 17.35 mA cm^{-2} and a FF of 57.1%), using a **Zn-26**:$PC_{61}BM$ ratio of 1:1 and pyridine and 1,8-diiodooctane as coadditives.

Chen and co-workers used Pd-mediated Sonogashira and Cu-mediated Ullmann cross-coupling reactions to synthesize porphyrin dimers **Zn29a,b** (Scheme 12).[37] The 5,15-dibrominated scaffolds **Zn-15c,f** reacted with a mixture of trimethylsilyl acetylene (TMSA) and triisopropylsilylacetylene (TIPSA), yielding the nonsymmetrical porphyrin ethynyl-substituted intermediate **Zn-27a,b**. Sequential selective deprotection of the TMS-protected ethynyl unit, followed by Sonogashira cross-coupling with *p*-iodo-*N*,*N*-dibutylaniline mediated by $Pd_2(dba)_3$, allowed the isolation of the nonsymmetrical monomeric porphyrins **Zn-28a,b** in excellent yields (82% and 90%). These monomeric porphyrins have then been used as templates to obtain porphyrin dimers **Zn-29a,b** under Ullmann cross-coupling reaction conditions after base-promoted deprotection of the TIPS-protected acetylenic unit. This sequential synthetic approach gave **Zn-29a** and **Zn-29b** in 70% and 80% yields, respectively.

A HOMO level trend of **Zn29b** (−5.11 eV) > **Zn29a** (−5.14 eV) > spiro-OMeTAD ≈ the monomeric **Zn-22a** (Scheme 10) (−5.22 eV) was observed in good line with the triple cation $Cs_{0.05}[(FA_{0.83}MA_{0.17})PbI_{0.83}Br_{0.17}]_{0.95}$ perovskite (−5.45 eV) for hole extraction. Both **Zn29a** (4.2×10^{-4} cm^2

https://doi.org/10.1021/acsomega.4c01961
ACS Omega 2024, 9, 31196−31219

Scheme 12. Synthetic Approach to Porphyrin-Based Dimers Zn-29a,b

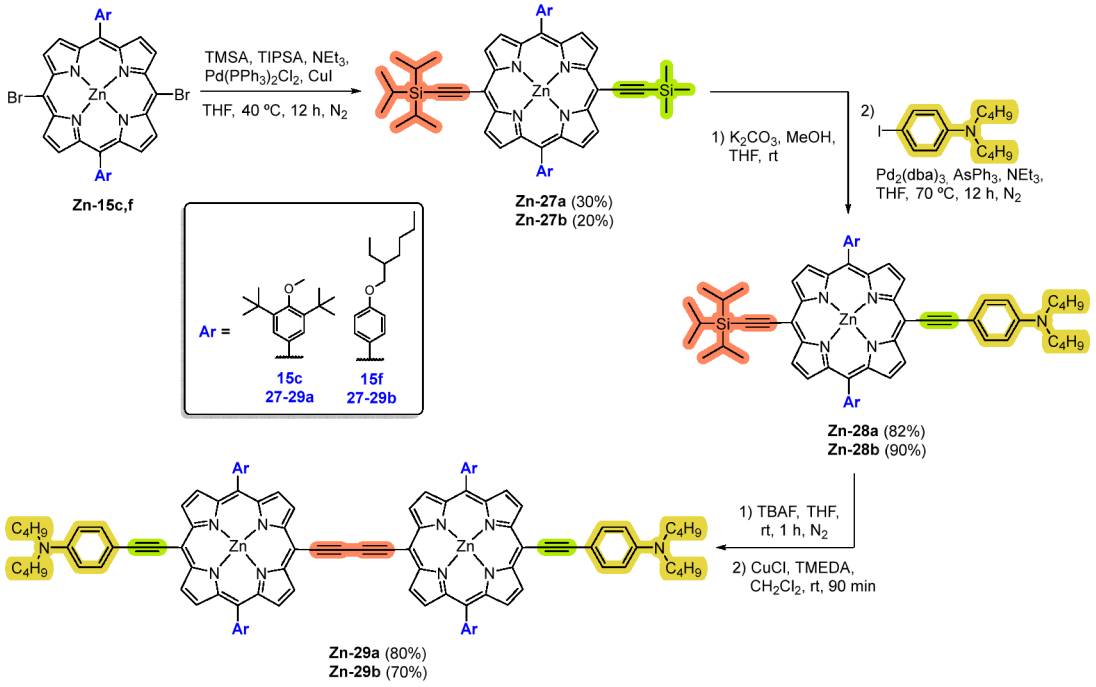

Scheme 13. Synthesis of 5,15-A_2B_2-type Porphyrin Derivatives Bearing Di- and Triarylamine Units

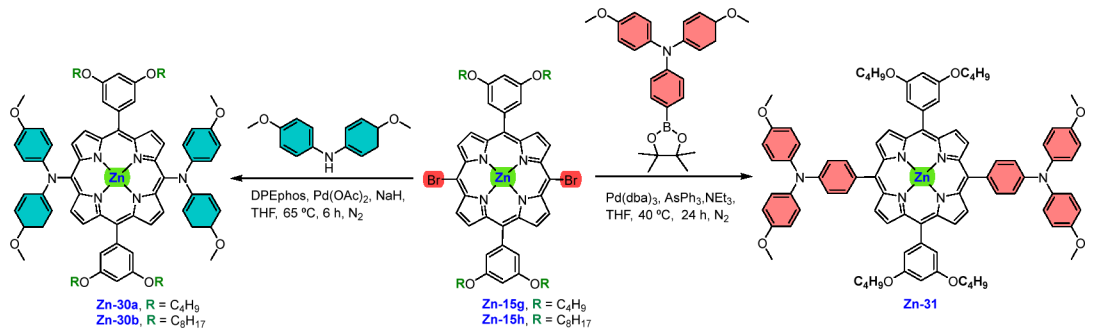

V^{-1} s^{-1}) and **Zn29b** (9.3×10^{-5} cm^2 V^{-1} s^{-1}) have higher hole mobility than monomeric porphyrin **Zn-22a** (3.2×10^{-5} cm^2 V^{-1} s^{-1}), ascribed to better intermolecular electronic coupling. The more appropriate linear peripheral functionalization in **Zn29a**, compared to the branched alkoxyl chains in **Zn29b**, provides better intermolecular $\pi-\pi$ packing for remarkable hole mobility, which is even better than that of spiro-OMeTAD (1.4×10^{-4} cm^2 V^{-1} s^{-1}). As expected, **Zn29a** in n-*i*-p mesoscopic devices demonstrated the highest PCE of 19.4% (V_{OC} = 1.096 V, J_{SC} = 22.60 mA cm^{-2}, and FF = 0.792), outperforming the spiro-OMeTAD with a PCE of 18.6% (V_{OC} = 1.086 V, J_{SC} = 22.64 mA cm^{-2}, and FF = 0.76). The **Zn29a**-based devices also exhibit better efficiency than the **Zn29b**-based device with a PCE of 17.84% and **Zn22a** contributing to a PCE of 17.93%. Furthermore, **Zn29a**-based devices exhibited better stability than their spiro-OMeTAD-based counterparts under moisture, light-soaking, and thermal testing conditions.

Gao reported the synthesis and the photovoltaic performance as HTM of the 5,15-A_2B_2-type derivatives **Zn-30** and **Zn-31** bearing di- and triarylamine units.[9] The synthetic approach involved the Pd(0)-mediated coupling of Zn(II) porphyrin complex **Zn-15g,h** with bis(4-methoxyphenyl)amine under Buchwald–Hartwig amination conditions or the Suzuki reaction with 4-methoxy-*N*-(4-methoxyphenyl)-*N*-(4-(4,4,5,5-tetramethyl-1,3,2-dioxaborolan-2-yl)phenyl)aniline (Scheme 13). Both palladium-catalyzed cross-coupling methods successfully generated porphyrin-arylamine derivatives **Zn-30a,b** and **Zn-31** in yields of *ca.* 62%.

This is the first example of the use of donor-π-donor porphyrins as HTM and structural features, such as the presence or absence of a phenyl spacer between the porphyrin core and the diarylamine moiety (**Zn-31** vs. **Zn-30a** and **Zn-30b**) as well as the size of the alkoxy-substituent at the 5,15-*meso* positions (**Zn-30a** and **Zn-31** vs. **Zn-30b**), to significantly impact performance. The direct porphyrin-diarylamine C–N bond in **Zn-30a** resulted in a n-*i*-p $FA_{0.8}MA_{0.2}PbI_3$-based PSC achieving a PCE of 22.67% with a V_{oc} of 1.135 V, J_{sc} of 24.56 mA cm^{-2}, and a FF of 0.81. This value far exceeded those obtained using **Zn-31** and **Zn-30b**, contributing to a PCE of 12.32% and 14.64%, respectively. Indeed, the energy level of **Zn-30a** is more favorable for charge transfer from the perovskite. Experimental hole mobility values of **Zn-30a** (4.23×10^{-3} cm^2 V^{-1} s^{-1}), **Zn-31** (1.46×10^{-3} cm^2 V^{-1} s^{-1}), and **Zn-30b** (1.24×10^{-3} cm^2 V^{-1} s^{-1}) and the worst morphology of the **Zn-30b** with the lengthy alkoxy leading to pinhole-filled films, to contribute for charge recombination at

https://doi.org/10.1021/acsomega.4c01961
ACS Omega 2024, 9, 31196–31219

perovskite-HTM interface, correlate highly with performances. Also, long-term stability studies showed that devices made from **Zn-30a** could maintain 89% of the initial PCE after 2000 h. A thermal stability test under 60% humidity and a temperature of 60 °C showed that the **Zn-30a**-based PSCs were able to retain 88% of initial efficiency after 360 h.

Reis et al. prepared a Zn(II) porphyrin complex incorporating carbazole units at 10,20-*meso* positions through a nucleophilic substitution reaction mediated by $PhI(OAc)_2$/$NaAuCl_4{\cdot}2H_2O$ (Scheme 14). The analogous Cu(II) was prepared using either an Ullmann or a Buchwald–Hartwig C–N transition-metal-assisted coupling.[38] Incorporation of carbazole units at the porphyrin was highly influenced by the electronic environment at the porphyrinic core. The Zn(II) complex showed metal replacement issues when the reaction was carried out under Pd-mediated Buchwald–Hartwig or Cu-mediated Ullmann conditions, resulting mainly in the exchange of Zn(II) with Pd(II) or Cu(II), respectively. However, oxidative nucleophilic substitution allowed the isolation of the porphyrin-carbazole Zn(II) complex **Zn-33** in 51% yield under mild conditions (Scheme 14).

Scheme 14. Synthesis of Zn(II) and Cu(II) Porphyrin-Carbazole Complexes

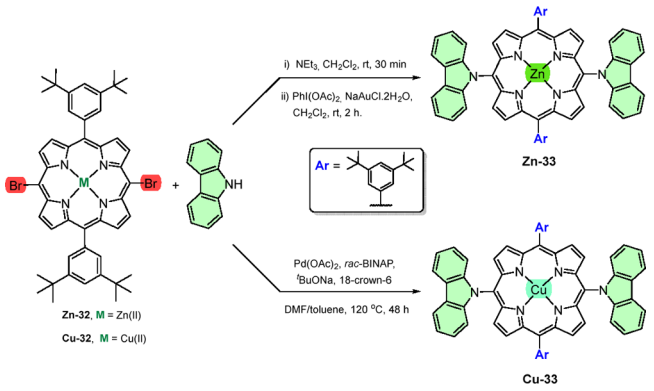

Cu(II) complex **Cu-33** was accomplished in 39% yield through the Pd(0)-promoted Buchwald–Hartwig cross-coupling reaction, since under oxidative nucleophilic substitution reaction or Ullmann conditions, the expected Cu(II) porphyrin-carbazole derivative was isolated in lower yields (11% and 31%, respectively) and the reaction took longer.

The HTM performance of the carbazole complexes **Zn-33** and **Cu-33** was systematically assessed in n–*i*–p mesoscopic $Cs_{0.05}[(FA_{0.83}MA_{0.17})PbI_{0.83}\ Br_{0.17}]_{0.95}$-based devices, doped with a 0.5/0.03/3.3 ratio of LiTFSI/FK209/TBP. The better alignment of HOMO energy level with the perovskite VB, together with HOMO electron density distribution located on the porphyrin core and carbazole units, placed the complex **Zn-33** as a more efficient HTM. In contrast, for Cu(II) complex **Cu-33** the HOMO is predominantly delocalized over the entire molecule. PSC devices using **Zn-33** achieved a PCE value of 9.87% (67% of the spiro-OMeTAD PCE = 14.7%),

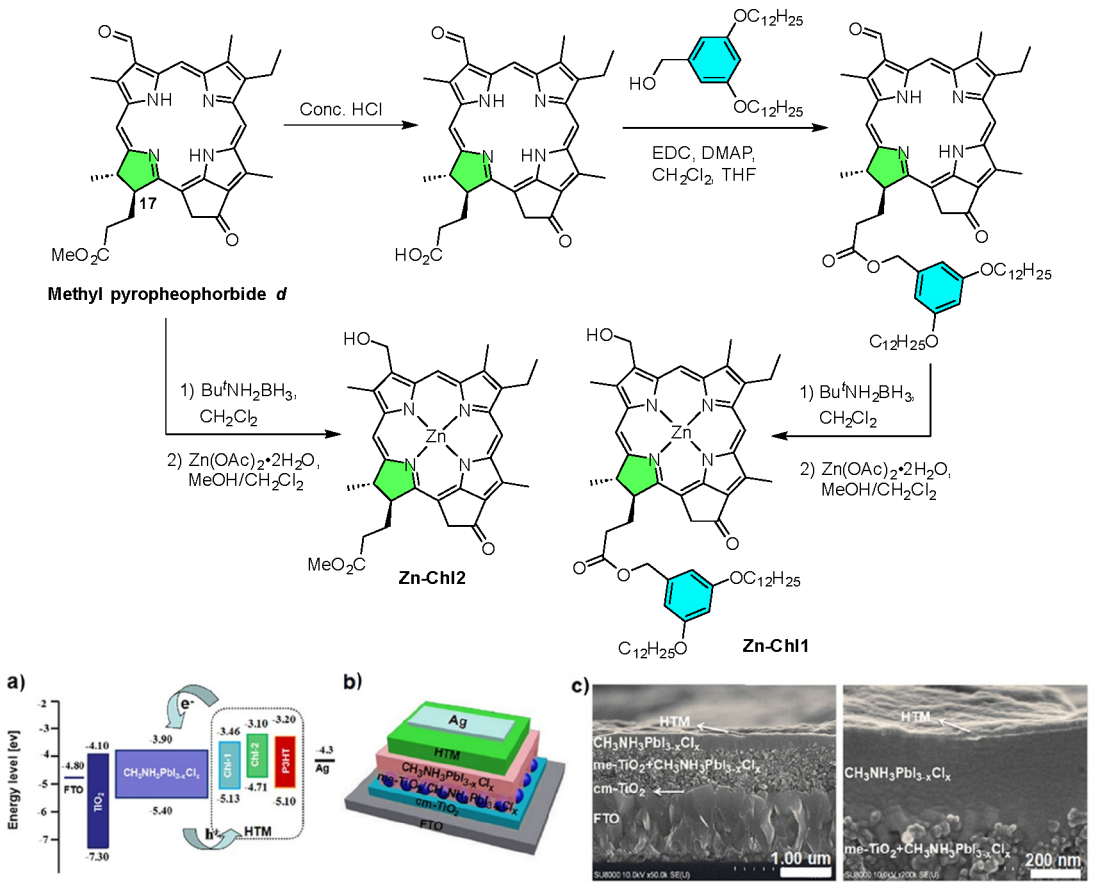

Figure 9. Synthetic pathway to obtain **Zn-Chl1** and **Zn-Chl2**. (a) Energy-level diagram, (b) architecture of PSC devices using chlorins **Zn-Chl1** and **Zn-Chl2** as HTM, and (c) PCE cross-section SEM pictures (figure adapted from ref 41 with permission from John Wiley and Sons).

https://doi.org/10.1021/acsomega.4c01961
ACS Omega 2024, 9, 31196–31219

Scheme 15. Synthetic Approach to Prepare BChl1−3 and Zn-BChl4 from Bacteriochlorophyll-*a*

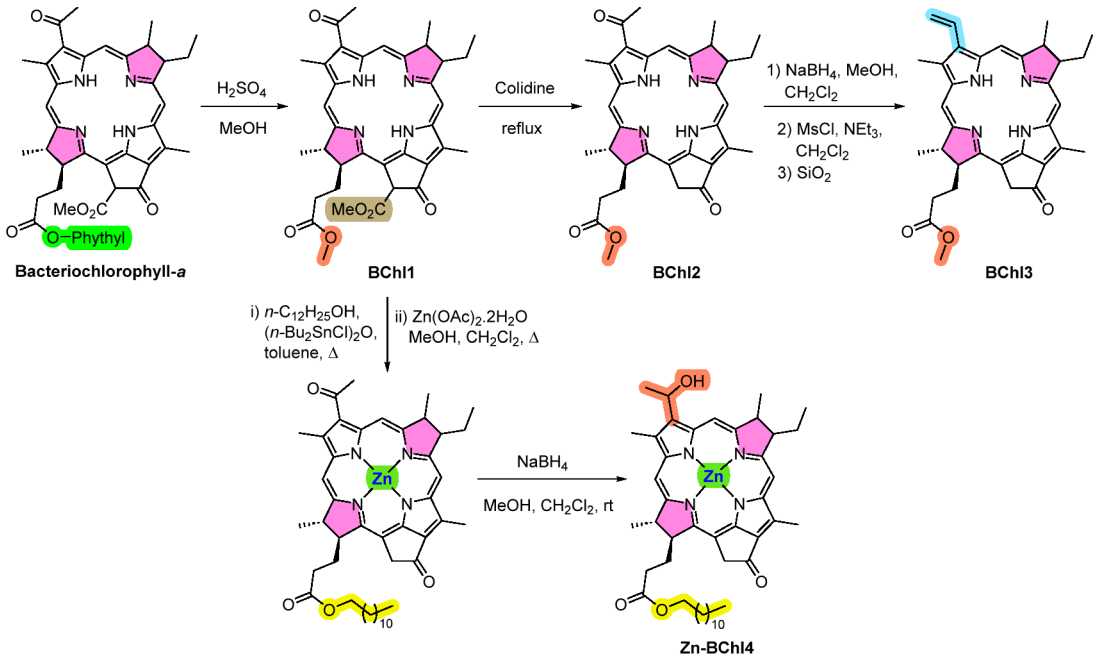

while **Cu-33** contributed to a PCE of 6.37%, similar to those obtained with the nonsubstituted precursors.

This study highlights the significance of the Zn(II) metal ion at the porphyrin core and the impact of the donor substituent at the *meso* positions, emphasizing the utility of directly attaching these units to the porphyrin core through C−N bonds.

PHOTOSYNTHETIC PIGMENTS AND ANALOGUES AS HTMs

Chlorophylls (Chl) and their analogues are getting attention from the scientific community as HTMs due to their abundance and crucial role in photosynthesis, dealing with tasks like absorbing light, energy transfer, and charge separation. The use in PSCs depends on the pigments' ability, along with their synthetic derivatives, to afford stacked supramolecular $\pi-\pi$ aggregates. In general, the self-assembly of these derivatives is driven by interactions involving hydroxyl and carbonyl functional groups as well metal ions present in the macrocycle core.[39,40]

In a study from 2016, Tian, Wang, and co-workers evaluated the potential use of Zn(II) complexes **Zn-Chl1** and **Zn-Chl2** as a HTM in PSCs with a n-*i*-p mesoscopic configuration. These complexes differed in the esterifying unit in the carboxyl functionality at position 17 (Figure 9).[41] Both derivatives were obtained from methyl pyropheophorbide-*d*,[42] and the access to **Chl1** required the acidic hydrolysis of the methyl ester function at position 17, followed by esterification with the adequate dodecyloxybenzyl alcohol under activating Steglich conditions. Then, the reduction of the formyl group to the corresponding alcohol was performed in the presence of the complex borane-*tert*-butylamine followed by metalation with $Zn(OAc)_2$ to afford **Zn-Chl1**. More directly, **Zn-Chl2** only required the reduction of the formyl group, followed by the metalation step.

$MAPbI_{3-x}Cl_x$ PSCs based on **Zn-Chl1** and **Zn-Chl2** without additives achieved efficiencies of 11.44% and 8.06%, respectively, while the controls obtained with conventional P3HT in the presence of dopants (LiTFSI and TBP) displayed an efficiency of 8.94% and with spiro-OMeTAD a value of 10.17%. The study confirmed the formation of **Chl** aggregates after spin-coating, and the superiority of **Chl1**-based devices was associated to lower-energy HOMO levels and crystalline films with smoother surfaces affording superior hole extraction efficiency and charge carrier mobility (Figure 9). Additionally, it was highlighted that the presence of dopants has a negative impact on the photovoltaic performance due to the partial disaggregation of the self-assembled *J*-aggregates, ascribed to their coordination to the central metal of **Zn-Chl1** and **Zn-Chl2**.

The potential of the related free-base bacteriochlorins **BChl1**, **BChl2**, and **BChl3** as HTM was also evaluated in PSCs with a n-*i*-p mesoscopic configuration using $MAPbI_3$ perovskite (Scheme 15).[43] These reduced derivatives were obtained from scaffold bacteriochlorophyll-*a* (**BChl-a**) after simultaneous demetalation and transesterification at position 17 using H_2SO_4 in methanol to give **BChl1**. Decarboxylation of the methoxycarbonyl unit at position 13[2] in refluxing 2,4,6-collidine afforded **BChl2** (methyl bacteriopyropheophorbide-*a*). The final **BChl3** with a vinyl group required reduction of the 3-acetyl group with $NaBH_4$ and subsequent mesylation of the hydroxy group to facilitate its elimination.[44]

Even without the structural features usually required for supramolecular assembly (*i.e.*, the hydroxy group at a peripheral position and the central metal ion on the macrocycle inner core), all these derivatives assembled as *J*-aggregates after spin-coating. In addition, **BChl1−3** exhibited a suitable HOMO level to mediate hole transfer. Even so, the best performance derived from **BChl2** bearing an acetyl functionality, with a PCE of 10.95% in the absence of dopants, followed by **BChl3** (4.85%) and then **BChl1** (1.30%). A result is associated with the better morphology of the **BChl2** aggregate film completely covering the perovskite surface. More significantly, unencapsulated **BChl2**-based devices maintained 80% of the PCE over 240 h at 20−30% humidity

https://doi.org/10.1021/acsomega.4c01961
ACS Omega 2024, 9, 31196−31219

Scheme 16. Synthetic Route to Zn-Chl3 and Zn-Por3 Derivatives

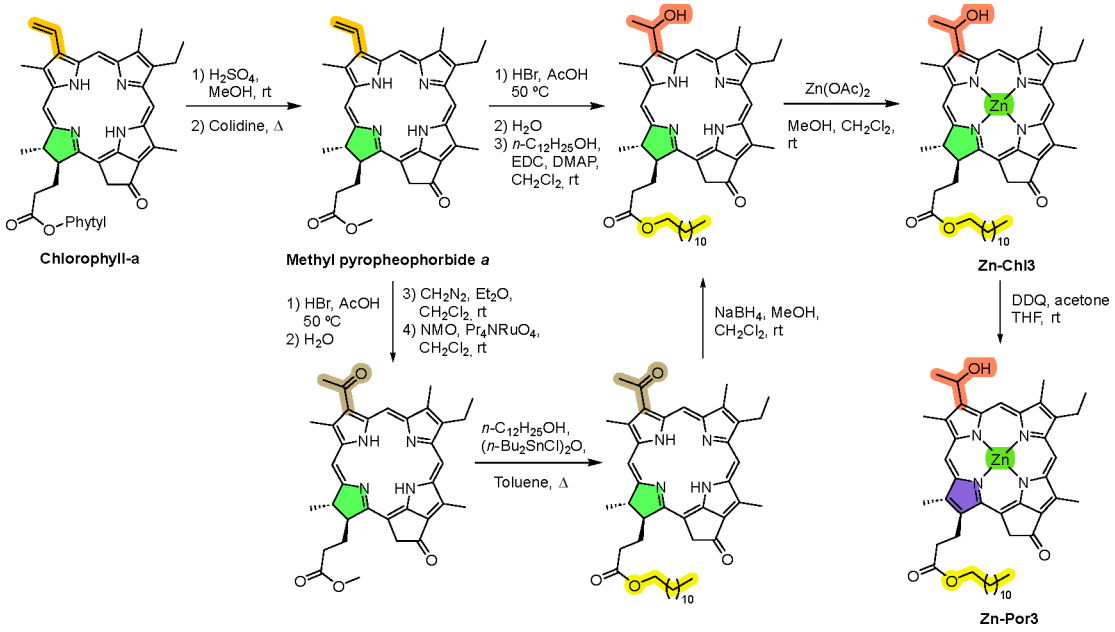

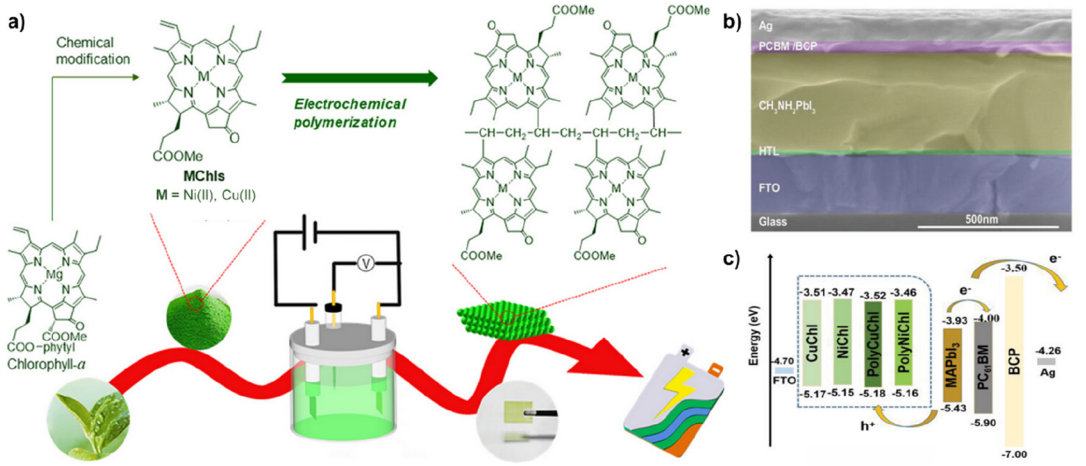

Figure 10. (a) Schematic representation of the preparation of **PolyCuChl** and **PolyNiChl** and their use as HTM in PSC devices; (b) cross-section structure of PSC devices and (c) energy-level diagram (figure adapted from ref 46 with permission from John Wiley and Sons).

and temperature of 0−15 °C, simulating also low-temperature conditions.

Studies were posteriorly conducted with **Zn-BChl4** (Scheme 15), **Zn-Chl3**, and **Zn-Por3** (Scheme 16) to evaluate the impact of oxidation state of the macrocycle backbone.[45] While **Zn-Chl3** and **Zn-Por3** were obtained from chlorophyll-*a*, **Zn-BChl4** arose from bacteriochlorophyll-*a*. In both approaches, the first step involved the simultaneous removal of the metal ion and transesterification of the carboxyl group at position 17, followed by a decarboxylation step at position 13[2]. Access to **Zn-BChl4**, after a second transesterification step with dodecanol and coordination with the Zn(II) metal ion, required the reduction of acetyl functionality with $NaBH_4$. The key step to reach **Zn-Chl3** was the hydrolysis of the vinyl group, followed by coordination with the metal ion. Instead, a multistep approach involving vinyl moiety oxidation, followed by transesterification and then a reduction step, can be performed. Oxidation of **Zn-Chl3** with DDQ provided **Zn-Por3**.

The PCE results using the $MAPbI_3$ perovskite allowed ordering the HTM efficiency as **Zn-Chl3** (11.88%) > **Zn-BChl4** (8.26%) and >**Zn-Por3** (0.68%). The performance of **Zn-BChl4**-based devices was limited by the higher HOMO energy-level distribution as well as imperfect *J*-aggregate formation. The small PCE of **Zn-Por3**-based PSCs has been attributed to the deeper HOMO level that produces a small energy gap between **Zn-Por3** and $MAPbI_3$ perovskite and also to the **Zn-Por3** roughness and delocalized aggregate structure of **Zn-Por3** at the **Zn-Por3**/$MAPbI_3$ interface to hinder hole transfer. The PCE of **Zn-Por3**-based PSCs was successfully improved to 4.04% by incorporating FA^+ and Br^- into the crystal lattice of $MAPbI_3$, downward from the perovskite VB.

Now, the exploration of **PolyCuChl** and **PolyNiChl** films obtained via the electrochemical polymerization of **CuChl** and **NiChl** (Figure 10a) for inverted based-$MAPbI_3$ PSC are the best outcomes reported with chlorophyll derivatives.[46] The authors selected methyl pyropheophorbide-*a* to prepare **CuChl** and **NiChl** monomers by metalation with adequate

https://doi.org/10.1021/acsomega.4c01961
ACS Omega 2024, 9, 31196−31219

Scheme 17. Synthetic Approach to Complex Zn-37

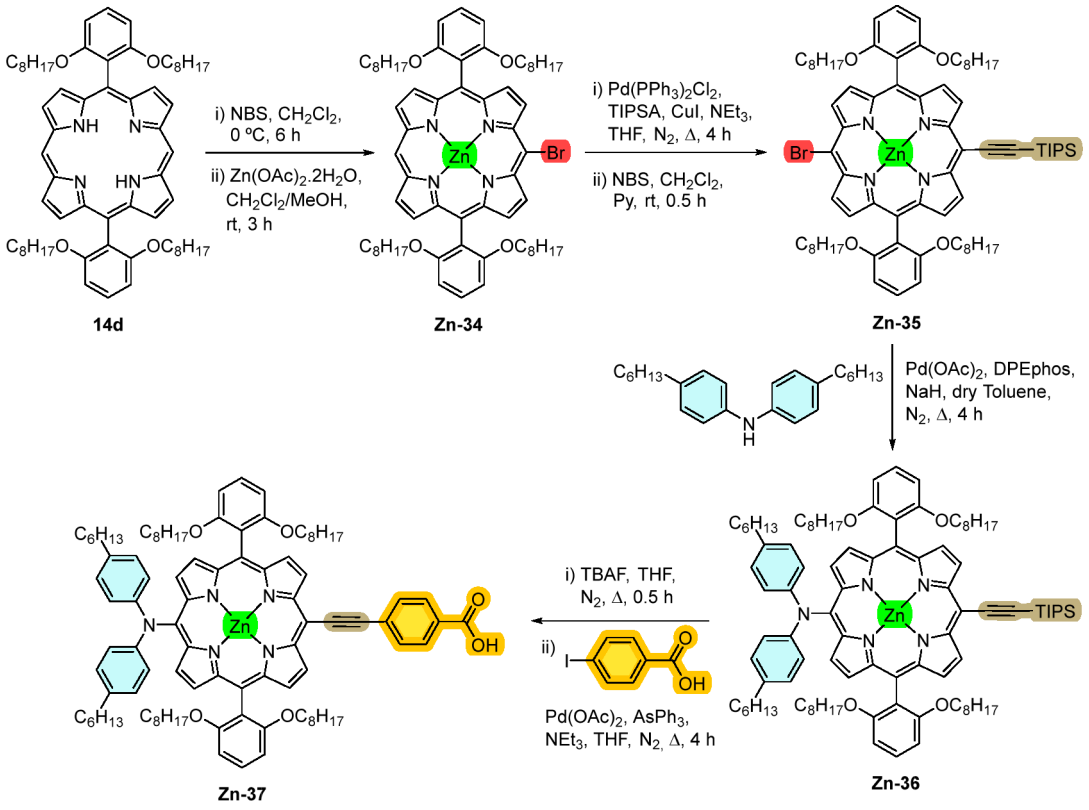

metal(II) acetate salt. Posteriorly, coupling of the peripheral vinyl group via electrochemical polymerization on the FTO glass afforded **PolyCuChl** and **PolyNiChl**. Compared to monomeric molecules, the chain polymeric structure effectively extends the intramolecular electron channels, allowing for high-speed charge transport, greatly enhancing hole collection ability, reducing charge complexation, and increasing the built-in voltage. As a result, spin-coated **CuChl** and **NiChl**-based PSCs exhibited PCE of 16.5% and 15.8%, respectively, while PSCs based on **PolyCuChl** and **PolyNiChl** HTM (Figure 10b,c) provided an improved PCE of 19.0% and 17.8%, respectively, with clear enhancements in V_{oc} and FF. Furthermore, unencapsulated devices based on **CuChl**, **NiChl**, **PolyCuChl**, and **PolyNiChl** exhibited high long-time stability and maintained 63%, 52%, 85%, and 88% of the original PCE, respectively, after storage in ambient air with a relative humidity of ≈20% for 1683 h.

■ PORPHYRINS AS DEFECT PASSIVATOR IMPROVING CHARGE TRANSPORT IN PSCs

Due to the soft ionic nature of perovskites, the crystallization process inevitably results in the formation of point defects along grain boundaries and on the surface. These defects act as trap states for photogenerated electrons and holes, hindering carrier dynamics and, thereby, degrading device performance. Moreover, they facilitate ion migration and diffusion within the material, exacerbating operational challenges. Additionally, these defects accelerate the moisture- and oxygen-induced degradation of perovskite materials. Of utmost importance is the perovskite/HTM interface, especially in n-*i*-p PSCs, where the misalignment of energy levels at this interface can lead to interfacial recombination losses, further compromising device efficiency. Overcoming these two critical aspects, the forthcoming works outline the synergistic effect of defect passivation and hole hopping of other HTMs arising from porphyrins, which plays a pivotal role in improving device stability and remains almost unexplored. Those porphyrins were incorporated into the perovskite film as an additive or employed as an interface material in the PSC device.

In 2019, Lin et al. reported that the quality of the perovskite film in n-*i*-p CsFAMA-based devices was improved in the presence of complex **Zn-37** used as an antisolvent additive.[47] This complex, described by Grätzel et al. in 2011 as a dye in DSSC devices, was obtained from porphyrin **14d** as outlined in Scheme 17.[48] Briefly, monobromination of **14d** with NBS, followed by metalation of the porphyrin inner core with $Zn(OAc)_2$, afforded **Zn-34** in 83% yield. Then, Sonogashira coupling with TIPSA and subsequent monobromination resulted in **Zn-35** in 85% yield. Finally, coupling of this intermediate with bis(4-hexylphenyl)amine under Buchwald–Hartwig conditions, followed by removal of the protecting TIPS group and reaction of **Zn-36** with 4-iodobenzoic acid under Sonogashira conditions, afforded the desired **Zn-37** in an overall yield of 77%.

DFT calculations suggested that **Zn-37**, with high charge density localized at the carboxylate, could coordinate/passivate the under-coordinated Pb^{2+} ions inside perovskite crystals, thus reducing the undesirable nonradiative charge recombination. In fact, X-ray photoelectron (XPS) measurements showed that the peaks located at 136.73 and 141.46 eV appearing in the control perovskite films and arising from the under-coordinated Pb^{2+} defects almost disappeared in the presence of **Zn-37**. Also, the increase of the VB of the modified perovskite material from −5.51 to −5.37 eV is another positive contribution to achieve the proper energy alignment for an adequate charge extraction. All this is in line with the best

https://doi.org/10.1021/acsomega.4c01961
ACS Omega 2024, 9, 31196−31219

performance of the modified devices with a PCE of 20.50% vs. a value of 18.5% for unmodified devices. The remarkably enhanced J_{sc} within **Zn-37** devices was ascribed to the increased light harvesting and improved charge separation and extraction because of the suppression of charge recombination by defect passivation. Besides, the existing hydrophobic alkyl chains improved the moisture stability of perovskite films. Consequently, unencapsulated PSCs based on **Zn-37** retain 93% of their initial PCE after storage in ambient air for 30 days (air 25−40 °C, 20−40% relative humidity) under dark conditions, whereas the PCE of unmodified devices drops to 74% after aging.

Gao et al. also observed that the donor-π-acceptor porphyrins **Zn38a−c** could effectively passivate the perovskite surface to improve cell performance as an interlayer between $FA_{0.8}MA_{0.2}PbI_3$ perovskite and the spiro-OMeTAD acting as HTL in n-*i*-p devices (Figure 11).[49] Starting with the same

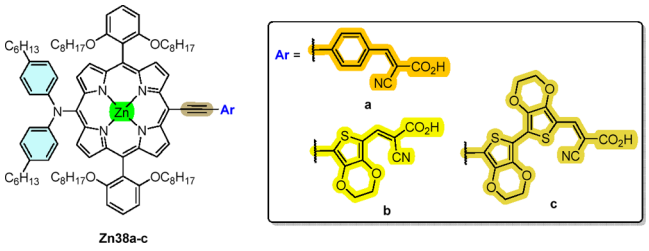

Figure 11. Structures of complexes **Zn38a−c**.

porphyrin **14d**, the authors used a synthetic methodology that differed from that reported by Li et al. only in the last steps.[47] After removal of the acetylene protecting group (TIPS) by TBAF, Sonogashira coupling with 2-cyano-3-(4-iodophenyl)-acrylic acid or 3-(6-bromo-7,8-ethylenedioxy-3-thiophene)-2-cyanoacrylic acid afforded complexes **Zn-38a** and **Zn-38b** in 85% and 73% yield, respectively. The synthesis of **Zn-38c**, obtained in 83% yield, required Sonogashira coupling with 5′-bromo-5-formyl-2,2′-bi(3,4-ethylenedioxythiophene), followed by a Knoevenagel condensation with cyanoacetic acid in the presence of piperidine.

As before, DFT calculations confirmed the location of negative charges in the carboxyl electron-withdrawing group. The characterization by XPS of each spin-coated film confirmed the presence of the porphyrin, and the lower binding energy found for Pb^{2+} demonstrated the passivation of undercoordinated Pb^{2+} defects. Moreover, the extension of the lifetimes from 16.64 ns for the control film to 26.72, 25.10, and 28.14 ns for the passivated samples with **Zn-38a**, **Zn-38b**, and **Zn-38c** confirmed inhibition of the recombination of carriers. As a result, devices treated with **Zn-38a**, **Zn-38b**, and **Zn-38c** showed PCE values of 22.14%, 22.37%, and 22.17%, respectively, whereas the best-performing control device achieved a PCE of 21.04%. Again, the improvement in V_{oc} (from 1.070 V for the control to 1.117 V for the **Zn38c**-treated device) and an FF of approximately 0.84 were attributed to the significant passivation effect and the improved perovskite/HTM interface. As before, the superior stability was associated to the hydrophobic character of the long alkyl chains present in the porphyrin core. Indeed, porphyrin-modified devices maintained around 93% of their initial PCE, while the control kept only 78.6% after 50 days under 30% humidity at room temperature without encapsulation.

Zhang et al. also reported an improvement in PSC devices (from 20.18% to 21.08%) when donor-π-acceptor complex **Zn-39** was used to passivate the perovskite film via the antisolvent process.[50] This *trans*-A_2B_2-type porphyrin was synthesized by the condensation of dipyrromethane **16** with pyridinecarboxaldehyde, followed by the metalation of the free-base with $Zn(OAc)_2$ (Scheme 18); in this synthetic pathway, the dipyrromethane was obtained in 65% yield, the free-base in 6.8% yield, and the metal complex in 91% yield.

The electrostatic potential map of **Zn-39** clearly indicated that the negative charges are mainly located on the N atom of the pyridine, and the expected coordination to the Pb^{2+} cations was confirmed by FTIR and XPS. Furthermore, the **Zn-39** in the perovskite layer acted as heterogeneous nucleation sites for the crystallization of 3D perovskite, improving the crystal formation and growth. Even more significantly, the photocarrier lifetime was more than three times longer than that of the control film. All this is reflected in improved performance of devices fabricated with **Zn-39** and attributed to the presence of bulky triarylamine in the porphyrin core that augments the steric hindrance to reduce the aggregation of porphyrin molecules, resulting then in an increase in V_{oc} and FF. Also, a better stability than the control device at 85 °C under N_2 atmosphere was achieved. After 1000 h of exposure to 50% humidity, the **Zn-39**-treated device showed a PCE loss inferior to 2%, while the control device showed a decrease higher than 10%.

It is well-established that thiol-based derivatives act as strong chelating agents toward Pb^{2+}. With this in mind, Cao and co-workers, in 2021, evaluated the efficiencies of PSC devices containing the complex **Cu-44** with an appended amino-ethanethiol unit as an interlayer between the perovskite film and the spiro-OMeTAD HTM (Scheme 19).[51] This compound was obtained from 5-(4-aminophenyl)-10,15,20-triphenylporphyrin **40**, and the synthetic approach required as the first step the alkylation of the amino group with 2-

Scheme 18. Synthetic Approach to Complex Zn-39

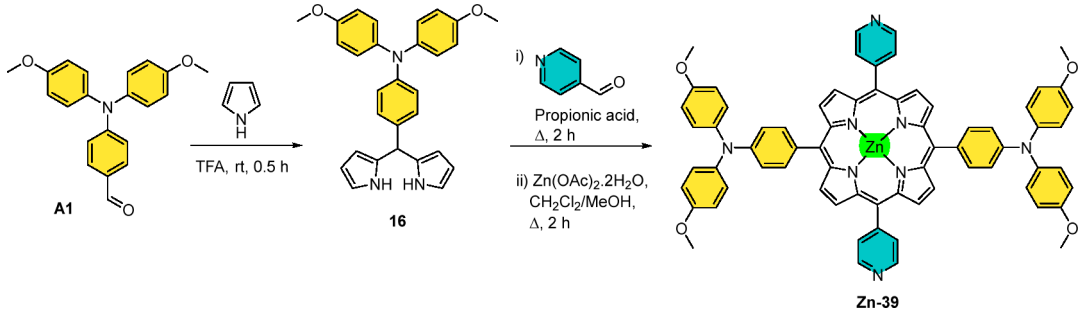

https://doi.org/10.1021/acsomega.4c01961
ACS Omega 2024, 9, 31196−31219

Scheme 19. Synthetic Approach to Cu-44

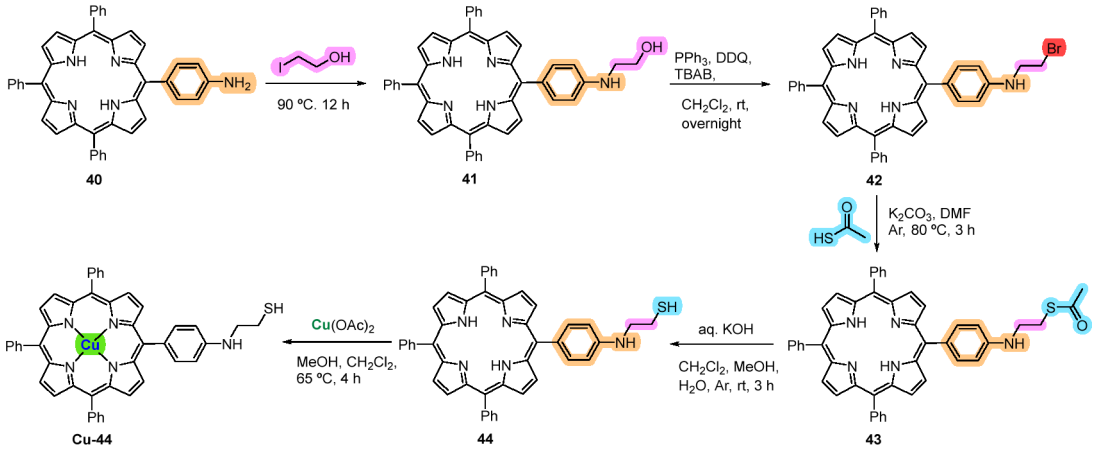

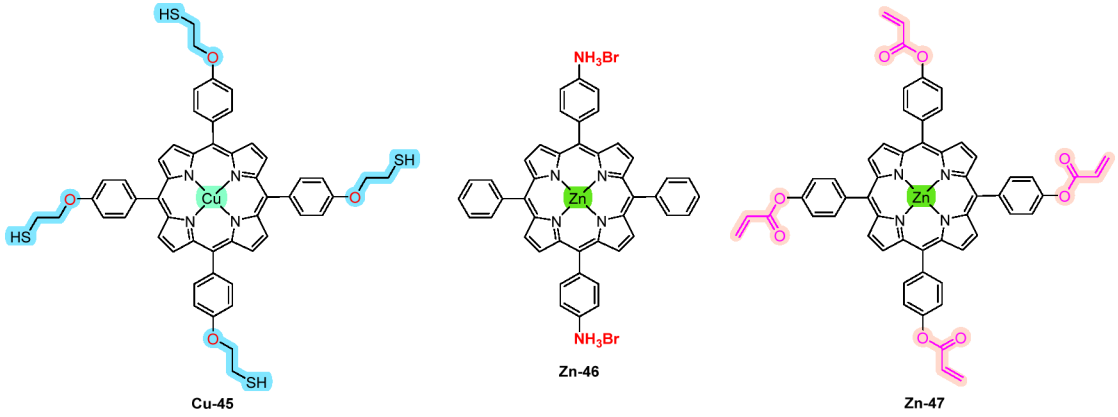

Figure 12. Structures of complexes **Cu-45**, **Zn-46**, and **Zn-47**.

iodoethanol, resulting in **41** in 62% yield. The reaction of this alcohol with tetrabutylammonium bromide (TBAB) in the presence of the PPh_3/DDQ system afforded bromide derivative **42** (76% yield), which after reaction with thiolacetic acid under basic conditions gave *N*-thioacetylated derivative **43** in 80% yield. Finally, this key intermediate after hydrolysis under basic conditions and coordination with $Cu(OAc)_2$ gave rise to required complex **Cu-44**.

The efficient modification of the perovskite surface with **Cu-44** was confirmed by XPS and the presence of Pb−S bonds by Raman spectroscopy; all of this attested to the ability of **Cu-44** to passivate Pb^{2+} defects. In addition, DFT calculations showed that the electron distribution within the porphyrin ring was tuned by the central Cu^{2+} ion and this could improve the fixation of I^-/I_2. Indeed, the IR spectrum of the **Cu-44**-treated perovskite validated the interaction between the *N*-H group of **Cu-44** and I^-/I_2. Furthermore, the surficial work function of the treated perovskite film improved to −5.2 eV, closer to spiro-OMeTAD, facilitating the interfacial charge transport. As a result, **Cu-44**-modified PSCs reached a PCE of 21.24%, while the best performance for untreated devices was 19.92%. More significantly, modified devices maintained over 90% of their original efficiency after 2000 h under AM 1.5G illumination, whereas reference cells retain only 10%.

In line with the previous work, the efficiency of $Cs_{0.05}(MA_{0.17}FA_{0.83})_{0.95}Pb(I_{0.83}Br_{0.17})_3$-based PSCs using complex **Cu-45** with four mercapto groups as an interlayer was also evaluated (Figure 12).[52] The synthetic methodology for **Cu-45** was similar to the former but using the 5,10,15,20-tetrakis[4-(2-bromoethoxy)phenyl]porphyrin as the starting scaffold.[51] As before, Pb−S bonds mediated the anchorage of **Cu-45** on the surface of the perovskite film. Photoluminescence (PL) results and space charge limited current (SCLC) measurements showed successful defect passivation. DFT calculations proved that the Cu(II) ion can effectively adjust the charge distribution of porphyrins, and the higher thermodynamic stability found for **Cu-45**−I^- than for **Cu-45**-I_2 corroborated the good fixation ability of the copper complex toward I^-. The results also showed that the HOMO level of **Cu-45** (−5.05 eV) has the required alignment with the VB of perovskite (−5.43 eV) for efficient charge transfer. With a PCE of 20.71%, the modified devices counterbalanced the value of 19.86% attained for pure perovskite-based cells. Moisture, thermal, and photostability were also improved. Going further, the authors also studied the impact of the porphyrin **45** as a free base and after being coordinated with Zn(II) ion. The best efficiency of PSCs with **Zn-45** was 20.41%, while that of free-base **45** resulted in a value of 20.11%. Indeed, the characterization of perovskite modified with **45**, **Cu-45**, and **Zn-45** confirmed the superiority of **Cu-45** to achieve the best film quality.

Feng et al. selected the conductive diammonium porphyrin **Zn-46** (Figure 12) to work as an interlayer on a CsMAFA-based perovskite film coated with $CsPbBr_3$ quantum dots (QDs).[53] Starting from the 5,15-bis(4-aminophenyl)-10,20-diphenylporphyrin and using a simple two-step synthetic

https://doi.org/10.1021/acsomega.4c01961
ACS Omega 2024, 9, 31196−31219

Scheme 20. Synthetic Approach Used to Obtain Dendrimer 49

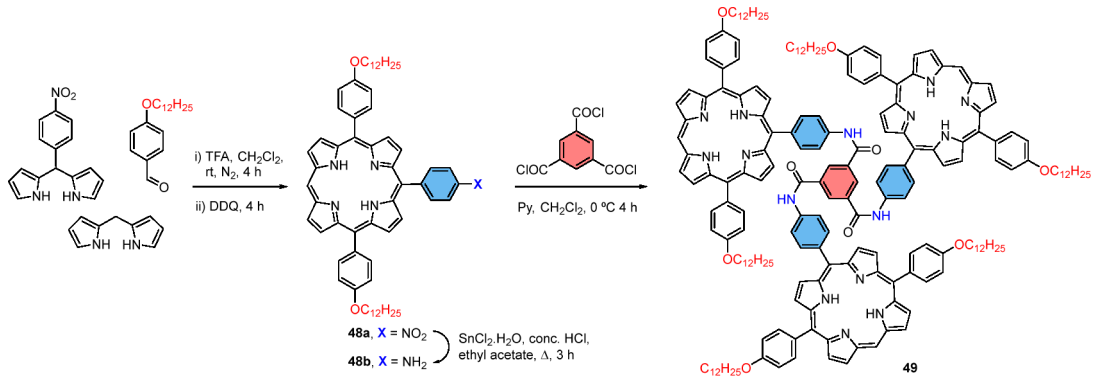

route—cationization and metalation with Zn(II)—the **Zn-46** was obtained in 85% yield.

Electrochemical results confirmed an adequate energy-level alignment for an efficient hole extraction [QD-**Zn-46** energy level (−5.38 eV) lower than the value of the perovskite (−5.5 eV) and higher than that of spiro-OMeTAD (−5.2 eV)]. Therefore, devices with the QD-**Zn-46** protecting layer exhibited improved charge recombination resistance (R_{cr}) than the control devices, leading to an increased V_{oc} and reduced charge-transfer resistance (R_{ct}). The result was the increase in PCE to 20.0% vs. 19.1% for PSCs fabricated without modification. More importantly, QD-**Zn-46**-based devices retained over 65 or 85% of original efficiency when tested at 85 °C or 45% humidity for 1000 h, respectively. Also, the QD-**Zn-46**-modified device kept 85% of its original efficiency after being exposed to AM 1.5 G illumination for 450 h.

Cao and co-workers also took advantage of the ability of porphyrin **Zn-47** (Figure 12) to polymerize *in situ* during the antisolvent process to form an active layer on top of $MAPbI_3$ perovskite with carbonyl groups to passivate defects and inhibit lead leakage.[54] The **Zn-47** was prepared by direct acylation of 5,10,15,20-tetrakis(4-hidroxyphenyl)porphyrin with acryloyl chloride in the presence of NEt_3. Metalation of free-base **47**, isolated in 22.5% yield, with $Zn(OAc)_2$ afforded **Zn-47**. The polymerization of **Zn-47** on the surface of the perovskite occurred at 150 °C and was attested by the shift of the C═O vibration peak in FTIR of $MAPbI_3$-**Zn-47**, while the coordination of Pb^{2+} was confirmed by XPS. Besides, the presence of $(\textbf{Zn-47})_n$ significantly suppressed the nonradiative recombination of photogenerated charge carriers. As a result, the PCE increased from 19.77% to 20.53%, with the most significant improvements in V_{oc} and FF characteristics. Finally, thermal stability studies confirmed that $(\textbf{Zn-47})_n$-based devices retained 77% of the initial PCE after 900 h at 85 °C, while in light stability studies retained 86% after 630 h at AM 1.5G. More significant has been the improved moisture stability at 45% humidity for 1800 h.

At the same time, Zhang et al. developed an effective interfacial material for surface passivation of $FA_{1-x}MA_xPbI_3$ perovskite film while enhancing the hole extraction ability at the perovskite/spiro-OMeTAD interface by using the free-base dendrimer **49** (Scheme 20).[55] The synthesis of **49** involved the acid-catalyzed condensation of 5-(4-nitrophenyl)-dipyrromethane, dipyrromethane, and 4-(dodecyloxy)-benzaldehyde, followed by DDQ oxidation, giving rise to the unsymmetric 5,15-di-(4-dodecyloxiphenyl)-10-(4-nitrophenyl)porphyrin **48a** in a yield of 7.6%. Treatment of **48a** with $SnCl_2$/HCl led to the reduction of the nitro group, resulting in **48b** in 79% yield. Finally, **49**, obtained in 52% yield, came from the reaction of **48b** with 1,3,5-benzene-tricarbonyl trichloride in the presence of pyridine.

The interaction of the carbonyl groups and also of the inner core of the free-base with Pb^{2+} ions was confirmed by FTIR and XPS. Most importantly, the strong $\pi-\pi$ aggregation of **49** in the perovskite film created a charge transfer channel facilitating the hole transfer between the perovskite and the HTM. As a result, a PCE of 22.30% was achieved, while the control device exhibited an efficiency of 21.30%. Indeed, decrease in PL intensity and longer lifetime compared to $FA_{1-x}MA_xPbI_3$/spiro-OMeTAD (95.12 ns vs. 90.5 ns) confirmed the successful dual role of **49** in increasing hole collection and reducing charge recombination at the interface. In addition, due to the strong intermolecular aggregation, unencapsulated **49**-treated devices retained 66% of their original PCE, while the control device dropped to 17% after 45 days' storage in ambient air (20 °C, 50−60% relative humidity) under dark conditions.

For this reason, Cao and co-workers modified perovskite materials adding the free-base 5-(4-aminophenyl)-10,15,20-triphenylporphyrin **40** (Scheme 19) or its metallic complexes [Co(II), Ni(II), Cu(II), or Zn(II)] (Figure 13) into the perovskite solution and compared the efficiency of the resulting devices.[56,57] In particular, the team discovered that self-assembly of the Ni(II)[56] or Cu(II)[57] complexes (**Ni-40** and **Cu-40**) into the $Cs_{0.05}Rb_{0.05}(FA_{0.83}MA_{0.17})_{0.90}Pb(I_{0.95}Br_{0.05})_3$ perovskite led to supramolecules that acted as passivators, improving charge transport within perovskite grain boundaries. In both cases, FAI and MABr cations protonate **M-40** [**M** = Ni(II) or Cu(II)] molecules, yielding ammonium **M-40H**$^+$ ions anchored on the perovskite grain surface that can effectively extract holes from the perovskite material due to the

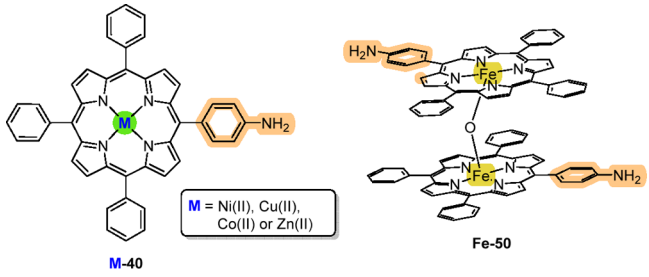

Figure 13. Structures of complexes **M-40** and the dimer **Fe-50**.

https://doi.org/10.1021/acsomega.4c01961
ACS Omega 2024, 9, 31196−31219

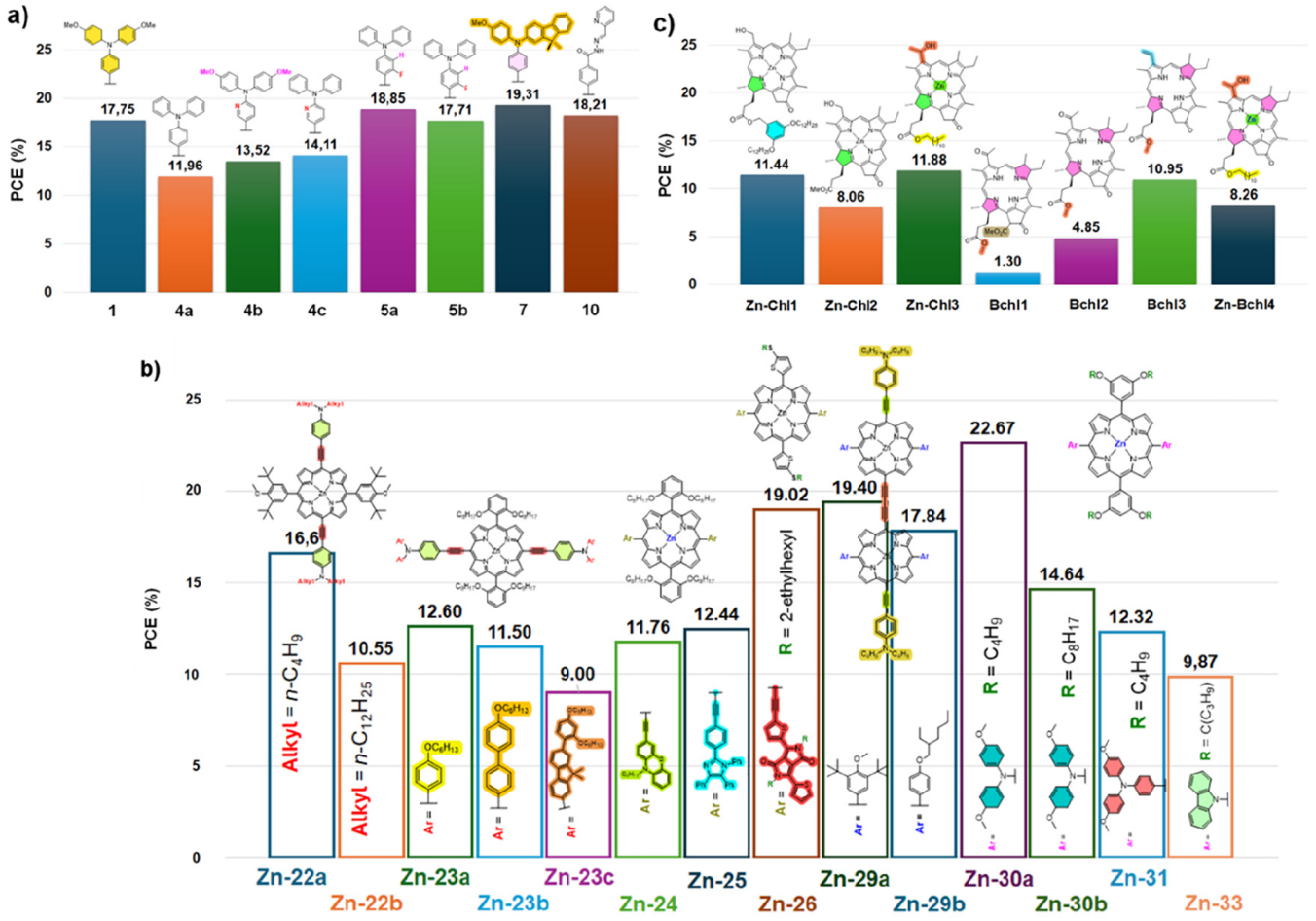

Figure 14. Maximum PCE values obtained with Zn(II) complexes of (a) A_4-type porphyrins, (b) *trans*-A_2B_2-type porphyrins, and (c) photosynthetic pigments as HTMs in PSCs.

strong intramolecular electric field along the direction of the ammonium side chain. All of this aligned with the best cell performance of PSC devices within porphyrin-supramolecules. These devices achieved a PCE of 24.2%, mainly originated from the improved V_{oc} and FF due to the more efficient charge extraction and transport in the perovskite film, while the average efficiency of control devices was around 22%. In fact, the doped films have higher hole mobility with 3.75×10^{-4} $cm^2\ V^{-1}\ s$ for **Ni-40** and 5.49×10^{-4} $cm^2\ V^{-1}\ s^{-1}$ for **Cu-40** vs. 1.58×10^{-4} $cm^2\ V^{-1}\ s^{-1}$ for pristine perovskite. Meanwhile, stability studies also confirmed that porphyrin-based PSC devices maintained 90% of the initial PCE value at room and higher temperatures (65 or 85 °C for Ni(II) and Cu(II), respectively) with high humidity after 3000 h. In contrast, reference PSC devices nearly failed stability tests.

In more recent work, Cao and collaborators also reported the remarkable increase in the hole mobility of a spiro-OMeTAD film (8-fold higher) after doping with oxygen-bridged dimer **Fe-50** (Figure 13). This improvement was ascribed to the formation of a one-dimensional supramolecular structure via $\pi-\pi$ interactions of adjacent dimers to reach large polarons on their oxygen bridges providing a sequential charge transfer on the HTM interface.[58] The synthesis of oxygen-bridged porphyrin dimer **Fe-50** was based on the treatment of 5-(4-aminophenyl)-10,15,20-triphenylporphyrin **40** with $FeCl_3$.

Although structural characterization of the **Fe-50**-doped spiro-OMeTAD films did not show any interaction between **Fe-50** and spiro-OMeTAD, the superior value for hole mobility when compared to the undoped spiro-OMeTAD film (3.17×10^{-4} versus 3.81×10^{-5} $cm^2\ V^{-1}\ s^{-1}$) and reduced decay time for **Fe-50**-doped spiro-OMeTAD (8.7 ns versus 16.5 ns for spiro-OMeTAD) corroborated the role of the interfacial transport channel provided by **Fe-50** in improving the hole mobility and promoting charge transport of the spiro-OMeTAD HTM. As a result, photovoltaic tests revealed that PSCs with **Fe-50** reached 23.2%, while the value for the device with pristine spiro-OMeTAD was 19.8%. As before, the **Fe-50**-doped device without encapsulation exhibited superior moisture stability by maintaining over 90% of the initial efficiency with ∼65% humidity after 3000 h. Under the same conditions, the pristine device decayed to 78% of its original performance, and the device with Li-TFSI doping dropped to below 40%. Again, the device based on **Fe-50** retained 90% of its initial efficiency after 1000 h at 85 °C with ∼30% humidity, while the device based on Li-TFSI lost over 80% of its original performance within 880 h. The device with **Fe-50** doping also revealed greatly improved photostability compared to the PSCs based on spiro-OMeTAD with and without Li-TFSI evaluated at AM 1.5 G illumination and ∼65 °C under a N_2 atmosphere.

https://doi.org/10.1021/acsomega.4c01961
ACS Omega 2024, 9, 31196−31219

FINAL REMARKS AND OUTLOOK

This review examines various synthetic strategies proposed by different research groups for developing porphyrin derivatives with the potential to be employed as a HTM in PSCs. Additionally, it explores some porphyrin derivatives that can act as defect passivators while improving charge transport. Those studies have shown that the performance and stability of the PSC devices are highly influenced by the nature of the substituents at the periphery of the macrocycle and by the metal ion at the porphyrin inner core. In general, the best device performances are associated with a better alignment of the porphyrin HOMO energy level with the perovskite valence band and improved film quality. Devices exhibiting higher stability and PCE values close to or even surpassing those of control devices based on conventional HTMs, such as spiro-OMeTAD and PTAA, suggest that porphyrin-based HTMs can become highly attractive for industrial applications.

From a synthetic perspective, the most appealing and cost-effective strategies are those leading to derivatives with an A_4-type core and electron-donating *meso*-substituents such as arylamines. These derivatives can be readily obtained in a single step or a maximum of two if metalation is necessary. The nonavailability of aldehydes needed for condensation with pyrrole does not represent a limitation as they can be obtained using simple approaches or highly efficient metal-catalyzed reactions like the Buchwald−Hartwig coupling, among others. Alternatively, the introduction of electron-donor units can be accomplished in the final steps by employing C−N coupling between the readily accessible 5,10,15,20-tetrakis(4-bromophenyl)porphyrin and the required amine under Buchwald−Hartwig conditions.

The HTMs obtained through the postfunctionalization of 5,15-A_2-porphyrins typically involve a multistep synthetic sequence. However, the high efficiency of metal-catalyzed reactions commonly employed in the envisaged strategy does not seem to compromise the synthetic protocol. More significantly, recent studies have demonstrated that direct functionalization of free-*meso* positions in 5,15-A_2-porphyrins with diarylamine moieties provides porphyrin HTMs with the best performance, achieving the highest PCE (22.67%) recorded currently.

The lesser attention given to HTMs based on photosynthetic pigments can be changed based on the excellent performance of films obtained from the electrochemical polymerization of the copper complex of methyl pyropheophorbide-*a*. The high abundance of the starting scaffolds and well-established protocols for obtaining the intermediates are positive factors supporting further investment in this category of HTM.

As summarized in Figure 14, HTMs based on A_4-type derivatives, bearing arylamine substituents at *meso* positions, exhibit consistent PCE values, while PCE values for *trans*-A_2B_2-type derivatives used as HTMs are more sensitive to the substituents, such as alkyl chain lengths and aromatic rings positioned between the nitrogen of the arylamine moiety and the porphyrin core. Concerning photosynthetic derivatives, the chlorin-based core seems to be a preferable choice as a HTM than the bacteriochlorin core (Figure 14c). However, in this case, deeper studies and further efforts are needed to enhance the ability and efficiency of this type of reduced derivative as HTMs in PSCs.

In addition, the presence of the heteroatoms O, S, and N in the substituents resulted in stronger interactions with the perovskite layer, leading to the passivation of lead and iodine defects on the surface and grain boundaries to improve crystal morphology and reach an outstanding perovskite film quality with high uniformity, thus reducing undesirable nonradiative charge recombination. As a result, the enhancement in PCE values for devices ranges between 1% to 2%, although porphyrins capable of organizing into a supramolecular structure via $\pi-\pi$ interactions achieved an increase surpassing 3%, providing a kind of charge transfer channel at the perovskite/HTM interface. The most effective dual effects, passivation of defects, and hole transportation from the perovskite layer to the spiro-OMeTAD were observed with porphyrins coordinated with Ni(II) or Cu(II) ions.

Also, porphyrins can effectively block water intrusion and ion release on the perovskite, contributing to the improved stability of the devices.

More significantly, porphyrin-based HTMs can offer solutions to several crucial challenges associated with PSCs. Exploring porphyrins with strong absorption beyond 800 nm is vital to complementing perovskite materials, significantly enhancing current density. Introducing hydrophobic groups, such as amide or ester side chains, can substantially improve the hydrophobicity. Additionally, combining porphyrins with fullerenes, single-walled carbon nanotubes, or graphene oxide can enhance the hole mobility and refine the electrical contact at the HTM/perovskite interface. More attention must be paid to the fact that doped HTMs generally exhibit much higher PCE than dopant-free counterparts due to improved charge transport properties. To eliminate the impact of lithium ions and balance between stability and efficiency, the use of other TFSI-based salts (*e.g.*, $ZnTFSI_2$, NaTFSI, AgTFSI), ionic liquids, and oxidative agents (*e.g.*, F4-TCNQ, F6-TCNNQ) as well as Lewis acid dopants, must be considered. Alternatively, the design of porphyrins with alkoxy groups could immobilize lithium ions. Additionally, incorporating phenylamine- or pyridine-based moieties into porphyrinic systems could eliminate the need for *tert*-butylpyridine additive. For future scalable applications, new deposition methods for the HTM layer are necessary to replace the nonscalable spin-coating method, which suffers from significant material waste. Thermal deposition has emerged as a promising alternative, with the planarity, conductivity, and glass transition temperature of porphyrins providing major advantages. Lastly, the high sensitivity of perovskites to moisture and the poor stability of PSC devices are significant limitations. Designing an HTM with dual effects of charge transportation and hydrophobicity emerges as a strategic solution, and undoubtedly, porphyrins are positioned as promising candidates for this purpose.

AUTHOR INFORMATION

Corresponding Authors

Ana M. V. M. Pereira − *LEPABE − Laboratory for Process Engineering, Environment, Biotechnology and Energy, Faculty of Engineering, University of Porto, 4200-465 Porto, Portugal; ALiCE − Associate Laboratory in Chemical Engineering, Faculty of Engineering, University of Porto, 4200-465 Porto, Portugal*; Email: mafaldapereira@fe.up.pt

Nuno M. M. Moura − *LAQV-Requimte and Department of Chemistry, University of Aveiro, 3010-193 Aveiro, Portugal*; orcid.org/0000-0002-9373-7006; Email: nmoura@ua.pt

https://doi.org/10.1021/acsomega.4c01961
ACS Omega 2024, 9, 31196−31219

Maria G. P. M. S. Neves − *LAQV-Requimte and Department of Chemistry, University of Aveiro, 3010-193 Aveiro, Portugal;* orcid.org/0000-0002-7953-8166; Email: gneves@ua.pt

Author

Melani J. A. Reis − *LAQV-Requimte and Department of Chemistry, University of Aveiro, 3010-193 Aveiro, Portugal*

Complete contact information is available at: https://pubs.acs.org/10.1021/acsomega.4c01961

Notes

The authors declare no competing financial interest.

Biographies

Melani J. A. Reis is a PhD student in Chemistry at the University of Aveiro since 2021. She completed her Master's degree in 2018 and her Bachelor's degree in 2016 both in Medicinal Chemistry and at the University of Beira Interior Faculty of Sciences, Portugal. She is coauthor of a patent and of several articles and communications in national and international scientific meetings. Presently her investigation is focused on the synthesis, functionalization, and characterization of porphyrins aiming to obtain new macrocycles with adequate features to be explored as hole-transporting material (HTM) in perovskite solar cells and as dyes in dye-sensitized solar cells.

Ana M. V. M. Pereira received her PhD degree in Chemistry at the University of Aveiro in 2009, working in synthetic methodologies for porphyrinoids. From 2010 to 2015, she worked as a bilateral postdoc at the University of Aveiro and Université de Strasbourg and led a national exploratory project focused on developing porphyrin-based dyes for dye-sensitized solar cells. Since 2016, she has been a researcher at LEPABE at the University of Porto. Her main interests include engineering technological aspects for highly efficient and long-lasting perovskite solar cells, as well developing solar redox flow devices. From 2019 to 2022, she was the leader of the project "PorphSol", which involved the University of Porto and the University of Aveiro, and aimed to design and evaluate new porphyrinoids to improve the efficiency of dye-sensitized solar cells and perovskite solar cells.

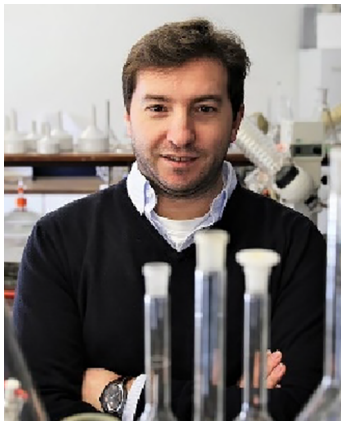

Nuno M. M. Moura got his BSc at the University of Évora in 2006 and received his PhD in Chemistry at the University of Aveiro in 2012. Since 2019, he is a researcher in LAQV-REQUIMTE, Department of Chemistry at the University of Aveiro. His research interests are focused on the development of synthetic approaches for the synthesis and modification of tetrapyrrolic macrocycles for potential application as photosensitizers in photodynamic therapy and antimicrobial photodynamic therapy, chemosensing, remediation, photocatalysis, and energy conversion systems. In recognition of his excellent work, he was awarded the "Portuguese Award for Best Young Organic Chemist" by the Portuguese Chemical Society.

Maria da Graça P. M. S. Neves is Associate Professor with Habilitation, at the Department of Chemistry, University of Aveiro, Portugal. She obtained her Habilitation and PhD degrees both at the University of Aveiro, her MSc degree at UMIST, Manchester, Great-Britain, and her BSc degree in Chemistry at the University of Lourenco Marques, Mozambique. Her research interests are centered on the synthesis and functionalization of tetrapyrrolic macrocycles (e.g., porphyrins, corroles, and phthalocyanines) for potential applications in photodynamic therapy, catalysis, chemical sensing, and solar cells.

■ ACKNOWLEDGMENTS

The authors thank the University of Aveiro, the University of Porto, and FCT/MCTES (PIDDAC) for financial support to the LAQV-REQUIMTE (LA/P/0008/2020, 10.54499/LA/P/0008/2020; UIDP/50006/2020, 10.54499/UIDP/50006/2020; and UIDB/50006/2020, 10.54499/UIDB/50006/

2020), LEPABE (UIDB/00511/2020, 10.54499/UIDP/00511/2020), and ALiCE (LA/P/0045/2020, 10.54499/LA/P/0045/2020) Research Units, and Portuguese NMR Network, through national funds. MJA Reis thanks FCT for her PhD grant (2020.05838.BD). AMVM Pereira thanks FCT and projects PorphSol (10.54499/PTDC/QUI-QOR/30357/2017) and ASAPFuels (10.54499/PTDC/EQU-EQU/4225/2021) for the research contracts and concession agreements. NMM Moura thanks FCT for funding through program DL 57/2016−Norma transitória (CDL-CTTRI-048-88-ARH/2018).

REFERENCES

(1) Nelson, J. *The Physics of Solar Cells;* Imperial College Press and Distributed by World Scientific Publishing Co., 2003.
(2) Kojima, A.; Teshima, K.; Shirai, Y.; Miyasaka, T. Organometal Halide Perovskites as Visible-Light Sensitizers for Photovoltaic Cells. *J. Am. Chem. Soc.* **2009**, *131* (17), 6050−6051.
(3) Zhu, P.; Chen, C.; Dai, J.; Zhang, Y.; Mao, R.; Chen, S.; Huang, J.; Zhu, J. Toward the Commercialization of Perovskite Solar Modules. *Adv. Mater.* **2024**, *36*, No. 2307357.
(4) Kim, J. Y.; Lee, J.-W.; Jung, H. S.; Shin, H.; Park, N.-G. High-Efficiency Perovskite Solar Cells. *Chem. Rev.* **2020**, *120* (15), 7867−7918.
(5) Zhu, W.; Wang, S.; Zhang, X.; Wang, A.; Wu, C.; Hao, F. Ion Migration in Organic−Inorganic Hybrid Perovskite Solar Cells: Current Understanding and Perspectives. *Small* **2022**, *18* (15), No. 2105783.
(6) Zhang, C.; Wei, K.; Hu, J.; Cai, X.; Du, G.; Deng, J.; Luo, Z.; Zhang, X.; Wang, Y.; Yang, L.; Zhang, J. A Review on Organic Hole Transport Materials for Perovskite Solar Cells: Structure, Composition and Reliability. *Mater. Today* **2023**, *67*, 518−547.
(7) Kadish, K. M.; Smith, K. M.; Guilard, R. *Handbook of Porphyrin Science;* World Scientific Publishing Company: Singapore, 2010.
(8) Chou, H.-H.; Chiang, Y.-H.; Li, M.-H.; Shen, P.-S.; Wei, H.-J.; Mai, C.-L.; Chen, P.; Yeh, C.-Y. Zinc Porphyrin−Ethynylaniline Conjugates as Novel Hole-Transporting Materials for Perovskite Solar Cells with Power Conversion Efficiency of 16.6%. *ACS Energy Lett.* **2016**, *1* (5), 956−962.
(9) Mai, C.; Xiong, Q.; Li, X.; Chen, J.; Chen, J.; Chen, C.; Xu, J.; Liu, C.; Yeh, C.; Gao, P. Thermally Stable D2h Symmetric Donor-π-Donor Porphyrins as Hole-Transporting Materials for Perovskite Solar Cells. *Angew. Chemie Int. Ed.* **2022**, *61* (39), No. e202209365.
(10) Urbani, M.; de la Torre, G.; Nazeeruddin, M. K.; Torres, T. Phthalocyanines and Porphyrinoid Analogues as Hole- and Electron-Transporting Materials for Perovskite Solar Cells. *Chem. Soc. Rev.* **2019**, *48* (10), 2738−2766.
(11) Matsuo, Y.; Ogumi, K.; Jeon, I.; Wang, H.; Nakagawa, T. Recent Progress in Porphyrin- and Phthalocyanine-Containing Perovskite Solar Cells. *RSC Adv.* **2020**, *10* (54), 32678−32689.
(12) Molina, D.; Follana-Berná, J.; Sastre-Santos, Á. Phthalocyanines, Porphyrins and Other Porphyrinoids as Components of Perovskite Solar Cells. *J. Mater. Chem. C* **2023**, *11* (24), 7885−7919.
(13) Chen, S.; Liu, P.; Hua, Y.; Li, Y.; Kloo, L.; Wang, X.; Ong, B.; Wong, W.-K.; Zhu, X. Study of Arylamine-Substituted Porphyrins as Hole-Transporting Materials in High-Performance Perovskite Solar Cells. *ACS Appl. Mater. Interfaces* **2017**, *9* (15), 13231−13239.
(14) Adler, A. D.; Longo, F. R.; Finarelli, J. D.; Goldmacher, J.; Assour, J.; Korsakoff, L. A Simplified Synthesis for Meso-Tetraphenylporphine. *J. Org. Chem.* **1967**, *32* (2), 476−476.
(15) Adler, A. D.; Longo, F. R.; Kampas, F.; Kim, J. On the Preparation of Metalloporphyrins. *J. Inorg. Nucl. Chem.* **1970**, *32* (7), 2443−2445.
(16) Shi, D.; Cao, Y.; Pootrakulchote, N.; Yi, Z.; Xu, M.; Zakeeruddin, S. M.; Grätzel, M.; Wang, P. New Organic Sensitizer for Stable Dye-Sensitized Solar Cells with Solvent-Free Ionic Liquid Electrolytes. *J. Phys. Chem. C* **2008**, *112* (44), 17478−17485.
(17) Shah, M. N.; Pathipati, S. R.; Ahmed, N. Porphyrin Based Hole Transport Layers for Enhanced Charge Transport and Stability in Perovskite Solar Cells. *J. Mater. Sci. Mater. Electron.* **2019**, *30* (8), 7866−7872.
(18) Lee, U.; Azmi, R.; Sinaga, S.; Hwang, S.; Eom, S. H.; Kim, T.; Yoon, S. C.; Jang, S.; Jung, I. H. Diphenyl-2-pyridylamine-Substituted Porphyrins as Hole-Transporting Materials for Perovskite Solar Cells. *ChemSusChem* **2017**, *10* (19), 3780−3787.
(19) Azmi, R.; Lee, U.-H.; Wibowo, F. T. A.; Eom, S. H.; Yoon, S. C.; Jang, S.-Y.; Jung, I. H. Performance Improvement in Low-Temperature-Processed Perovskite Solar Cells by Molecular Engineering of Porphyrin-Based Hole Transport Materials. *ACS Appl. Mater. Interfaces* **2018**, *10* (41), 35404−35410.
(20) Pudi, R.; Rodríguez-Seco, C.; Vidal-Ferran, A.; Ballester, P.; Palomares, E. *o,p*-Dimethoxybiphenyl Arylamine Substituted Porphyrins as Hole-Transport Materials: Electrochemical, Photophysical, and Carrier Mobility Characterization. *Eur. J. Org. Chem.* **2018**, *2018* (18), 2064−2070.
(21) Lindsey, J. S.; Schreiman, I. C.; Hsu, H. C.; Kearney, P. C.; Marguerettaz, A. M. Rothemund and Adler-Longo Reactions Revisited: Synthesis of Tetraphenylporphyrins under Equilibrium Conditions. *J. Org. Chem.* **1987**, *52* (5), 827−836.
(22) Wang, Y.-D.; Shao, J.-Y.; Lan, Z.-R.; Zhong, Y.-W. Fluorene-Modified Zinc Porphyrin as Low-Cost Hole-Transporting Material for Efficient Perovskite Solar Cells. *Org. Mater.* **2022**, *4* (02), 28−35.
(23) Lan, Y.; Wang, Y.-D.; Lan, Z.-R.; Wang, Y.; Cui, B.-B.; Shao, J.-Y.; Zhong, Y.-W. Thermally Stable Inverted Perovskite Solar Cells Using an Electropolymerized Zn-Porphyrin Film as a Dopant-Free Hole-Transporting Layer. *J. Mater. Chem. A* **2023**, *11* (13), 7085−7093.
(24) Wu, Y.; Zhang, Q.; Liu, J.-C.; Li, R.-Z.; Jin, N.-Z. A Novel Self-Assembly with Two Acetohydrazide Zinc Porphyrins Coordination Polymer for Supramolecular Solar Cells. *Org. Electron.* **2017**, *41*, 301−306.
(25) Lv, X.; Xiao, G.; Feng, X.; Cao, J.; Yao, X.; Liu, J. Acylhydrazone-Based Porphyrin Derivative as Hole Transport Material for Efficient and Thermally Stable Perovskite Solar Cells. *Dyes Pigments* **2019**, *160*, 957−961.
(26) Si, C.-D.; Lv, X.-D.; Long, S.-J. Perovskite Solar Cells Employing Copper (I/II) Porphyrin Hole-Transport Material with Enhanced Performance. *Inorg. Chem. Commun.* **2020**, *112*, No. 107701.
(27) Lindsey, J. S.; Hsu, H. C.; Schreiman, I. C. Synthesis of Tetraphenylporphyrins under Very Mild Conditions. *Tetrahedron Lett.* **1986**, *27* (41), 4969−4970.
(28) Sygkridou, D.; Apostolopoulou, A.; Charisiadis, A.; Nikolaou, V.; Charalambidis, G.; Coutsolelos, A. G.; Stathatos, E. New Metal−Free Porphyrins as Hole−Transporting Materials in Mesoporous Perovskite Solar Cells. *ChemistrySelect* **2018**, *3* (9), 2536−2541.
(29) Cao, J.; Lv, X.; Zhang, P.; Chuong, T. T.; Wu, B.; Feng, X.; Shan, C.; Liu, J.; Tang, Y. Plant Sunscreen and Co(II)/(III) Porphyrins for UV-Resistant and Thermally Stable Perovskite Solar Cells: From Natural to Artificial. *Adv. Mater.* **2018**, *30* (27), No. 1800568.
(30) Zhang, W.; Hua, Y.; Wang, L.; Zhang, B.; Li, Y.; Liu, P.; Leandri, V.; Guo, Y.; Chen, H.; Gardner, J. M.; Sun, L.; Kloo, L. The Central Role of Ligand Conjugation for Properties of Coordination Complexes as Hole-Transport Materials in Perovskite Solar Cells. *ACS Appl. Energy Mater.* **2019**, *2* (9), 6768−6779.
(31) Chou, H.-H.; Chiang, Y.-H.; Chen, Y.-H.; Guo, C.-J.; Zuo, H.-Y.; Cheng, W.-T.; Lin, P.-Y.; Chiu, Y.-Y.; Chen, P.; Yeh, C.-Y. Porphyrin-Based Simple and Practical Dopant-Free Hole-Transporting Materials for Efficient Perovskite Solar Cells Using TiO_2 Semiconductors. *Sol. RRL* **2020**, *4* (9), No. 2000119.
(32) Kang, S. H.; Lu, C.; Zhou, H.; Choi, S.; Kim, J.; Kim, H. K. Novel π-Extended Porphyrin-Based Hole-Transporting Materials with Triarylamine Donor Units for High Performance Perovskite Solar Cells. *Dyes Pigments* **2019**, *163*, 734−739.

https://doi.org/10.1021/acsomega.4c01961
ACS Omega 2024, 9, 31196−31219

(33) Reddy, G.; Katakam, R.; Devulapally, K.; Jones, L. A.; Della Gaspera, E.; Upadhyaya, H. M.; Islavath, N.; Giribabu, L. Ambient Stable, Hydrophobic, Electrically Conductive Porphyrin Hole-Extracting Materials for Printable Perovskite Solar Cells. *J. Mater. Chem. C* **2019**, *7* (16), 4702−4708.
(34) Reddy, G.; Basak, P.; Jones, L. A.; Della Gaspera, E.; Islavath, N.; Giribabu, L. Crystalline D-π-D Porphyrin Molecules as a Hole-Transporting Material for Printable Perovskite Solar Cells. *Sol. Energy* **2020**, *206*, 539−547.
(35) Devulapally, K.; Chowdhury, T. H.; He, Y.; Rajesh, M. N.; Prasanthkumar, S.; Islam, A.; Giribabu, L. Triphenylimidazole Substituted D-π-D Porphyrin Based Dopant-Free Hole Transport Materials for Perovskite Solar Cells. *J. Photochem. Photobiol.* **2023**, *16*, No. 100188.
(36) Gao, K.; Zhu, Z.; Xu, B.; Jo, S. B.; Kan, Y.; Peng, X.; Jen, A. K.-Y. Highly Efficient Porphyrin-Based OPV/Perovskite Hybrid Solar Cells with Extended Photoresponse and High Fill Factor. *Adv. Mater.* **2017**, *29* (47), No. 1703980.
(37) Chiang, Y.-H.; Chou, H.-H.; Cheng, W.-T.; Li, Y.-R.; Yeh, C.-Y.; Chen, P. Porphyrin Dimers as Hole-Transporting Layers for High-Efficiency and Stable Perovskite Solar Cells. *ACS Energy Lett.* **2018**, *3* (7), 1620−1626.
(38) Reis, M. J. A.; Nogueira, A. T.; Eulálio, A.; Moura, N. M. M.; Rodrigues, J.; Ivanou, D.; Abreu, P. E.; Correia, M. R. P.; Neves, M. G. P. M. S.; Pereira, A. M. V. M.; Mendes, A. C−N Linked Donor Type Porphyrin Derivatives: Unrevealed Hole-Transporting Materials for Efficient Hybrid Perovskite Solar Cells. *Dalt. Trans.* **2023**, *52* (41), 14762−14773.
(39) Patwardhan, S.; Sengupta, S.; Siebbeles, L. D. A.; Würthner, F.; Grozema, F. C. Efficient Charge Transport in Semisynthetic Zinc Chlorin Dye Assemblies. *J. Am. Chem. Soc.* **2012**, *134* (39), 16147−16150.
(40) Sengupta, S.; Würthner, F. Chlorophyll J-Aggregates: From Bioinspired Dye Stacks to Nanotubes, Liquid Crystals, and Biosupramolecular Electronics. *Acc. Chem. Res.* **2013**, *46* (11), 2498−2512.
(41) Li, M.; Li, Y.; Sasaki, S.; Song, J.; Wang, C.; Tamiaki, H.; Tian, W.; Chen, G.; Miyasaka, T.; Wang, X. Dopant-Free Zinc Chlorophyll Aggregates as an Efficient Biocompatible Hole Transporter for Perovskite Solar Cells. *ChemSusChem* **2016**, *9* (19), 2862−2869.
(42) Huber, V.; Sengupta, S.; Würthner, F. Structure−Property Relationships for Self-Assembled Zinc Chlorin Light-Harvesting Dye Aggregates. *Chem. - A Eur. J.* **2008**, *14* (26), 7791−7807.
(43) Li, M.; Sasaki, S.; Sanehira, Y.; Miyasaka, T.; Tamiaki, H.; Ikeuchi, T.; Chen, G.; Wang, X.-F. Biosupramolecular Bacteriochlorin Aggregates as Hole-Transporters for Perovskite Solar Cells. *J. Photochem. Photobiol. A Chem.* **2018**, *353*, 639−644.
(44) Sasaki, S.; Tamiaki, H. Synthesis and Optical Properties of Bacteriochlorophyll- a Derivatives Having Various C3 Substituents on the Bacteriochlorin π-System. *J. Org. Chem.* **2006**, *71* (7), 2648−2654.
(45) Li, M.; Li, N.; Hu, W.; Chen, G.; Sasaki, S.; Sakai, K.; Ikeuchi, T.; Miyasaka, T.; Tamiaki, H.; Wang, X.-F. Effects of Cyclic Tetrapyrrole Rings of Aggregate-Forming Chlorophyll Derivatives as Hole-Transporting Materials on Performance of Perovskite Solar Cells. *ACS Appl. Energy Mater.* **2018**, *1* (1), 9−16.
(46) Liu, Z.; Zhang, C.; Yang, L.; Xiang, T.; Li, N.; Li, A.; Sun, Y.; Ren, H.; Sasaki, S.; Miyasaka, T.; Wang, X. Perovskite Solar Cells Based on Polymerized Chlorophyll Films as Environmentally Friendly Hole-Transporting Layers. *Small* **2024**, *20*, 2305484.
(47) Zhou, Y.; Zhong, H.; Han, J.; Tai, M.; Yin, X.; Zhang, M.; Wu, Z.; Lin, H. Synergistic Effect of Charge Separation and Defect Passivation Using Zinc Porphyrin Dye Incorporation for Efficient and Stable Perovskite Solar Cells. *J. Mater. Chem. A* **2019**, *7* (46), 26334−26341.
(48) Yella, A.; Lee, H.-W.; Tsao, H. N.; Yi, C.; Chandiran, A. K.; Nazeeruddin, M. K.; Diau, E. W.-G.; Yeh, C.-Y.; Zakeeruddin, S. M.; Grätzel, M. Porphyrin-Sensitized Solar Cells with Cobalt (II/III)−Based Redox Electrolyte Exceed 12% Efficiency. *Science (80-.).* **2011**, *334* (6056), 629−634.
(49) Mai, C.; Zhou, Q.; Xiong, Q.; Chen, C.; Xu, J.; Zhang, Z.; Lee, H.; Yeh, C.; Gao, P. Donor−π−Acceptor Type Porphyrin Derivatives Assisted Defect Passivation for Efficient Hybrid Perovskite Solar Cells. *Adv. Funct. Mater.* **2021**, *31* (7), No. 2007762.
(50) Su, K.; Chen, W.; Huang, Y.; Yang, G.; Brooks, K. G.; Zhang, B.; Feng, Y.; Nazeeruddin, M. K.; Zhang, Y. In Situ Graded Passivation via Porphyrin Derivative with Enhanced Photovoltage and Fill Factor in Perovskite Solar Cells. *Sol. RRL* **2022**, *6* (4), No. 2100964.
(51) Li, C.; Wang, L.; Yan, P.-J.; Liu, H.; Cao, J.; Chen, C.-C.; Tang, Y. Perovskite Surface Management by Thiol and Amine Copper Porphyrin for Stable and Clean Solar Cells. *Chem. Eng. J.* **2021**, *409*, No. 128167.
(52) Yan, P.; Cao, J.; Pang, J.; Yang, Z.; Wang, X.; Yao, X. Chemical Encapsulation of Perovskite Film by Tetra-Thiol Copper(II) Porphyrin for Stable and Clean Photovoltaics. *Org. Electron.* **2021**, *93*, No. 106158.
(53) Feng, X.-X.; Lv, X.-D.; Liang, Q.; Cao, J.; Tang, Y. Diammonium Porphyrin-Induced $CsPbBr_3$ Nanocrystals to Stabilize Perovskite Films for Efficient and Stable Solar Cells. *ACS Appl. Mater. Interfaces* **2020**, *12* (14), 16236−16242.
(54) Liang, H.; Wang, W. D.; Mai, S.; Lv, X.; Fang, J.; Cao, J. Lead Fixation by Spider Web-like Porphyrin Polymer for Stable and Clean Perovskite Solar Cells. *Chem. Eng. J.* **2022**, *429*, No. 132405.
(55) Su, K.; Zhao, P.; Ren, Y.; Zhang, Y.; Yang, G.; Huang, Y.; Feng, Y.; Zhang, B. A Porphyrin-Involved Benzene-1,3,5-Tricarboxamide Dendrimer (Por-BTA) as a Multifunctional Interface Material for Efficient and Stable Perovskite Solar Cells. *ACS Appl. Mater. Interfaces* **2021**, *13* (12), 14248−14257.
(56) Fang, Z.; Wang, L.; Mu, X.; Chen, B.; Xiong, Q.; Wang, W. D.; Ding, J.; Gao, P.; Wu, Y.; Cao, J. Grain Boundary Engineering with Self-Assembled Porphyrin Supramolecules for Highly Efficient Large-Area Perovskite Photovoltaics. *J. Am. Chem. Soc.* **2021**, *143* (45), 18989−18996.
(57) Zhao, J.; Mu, X.; Wang, L.; Fang, Z.; Zou, X.; Cao, J. Homogeneously Large Polarons in Aromatic Passivators Improves Charge Transport between Perovskite Grains for >24% Efficiency in Photovoltaics. *Angew. Chemie Int. Ed.* **2022**, *61* (14), No. e202116308.
(58) Mu, X.; Liu, Y.; Xiao, G.; Xu, C.; Gao, X.; Cao, J. Porphyrin Supramolecule as Surface Carrier Modulator Imparts Hole Transporter with Enhanced Mobility for Perovskite Photovoltaics. *Angew. Chemie Int. Ed.* **2023**, *62* (39), No. e202307152.

https://doi.org/10.1021/acsomega.4c01961
ACS Omega 2024, 9, 31196−31219